USGS
science for a changing world

FEMA

Report from USGS to FEMA for Interagency Agreement HSFE09-15-X-0805 (DR-4193)

Key Recovery Factors for the August 24, 2014, South Napa Earthquake

By Kenneth W. Hudnut, Thomas M. Brocher, Carol S. Prentice, John Boatwright, Benjamin A. Brooks, Brad T. Aagaard, J. Luke Blair, Joe B. Fletcher, Jemile E. Erdem, Charles W. Wicks, Jessica R. Murray, Fred F. Pollitz, John Langbein, Jerry Svarc, David P. Schwartz, Daniel J. Ponti, Suzanne Hecker, Stephen DeLong, Carla Rosa, Brenda Jones, Rynn Lamb, Anne M. Rosinski, Timothy P. McCrink, Timothy E. Dawson, Gordon Seitz, Ron S. Rubin, Craig Glennie, Darren Hauser, Todd Ericksen, Dan Mardock, Don F. Hoirup, and Jonathan D. Bray

Open-File Report 2014–1249

U.S. Department of the Interior
U.S. Geological Survey

U.S. Department of the Interior
SALLY JEWELL, Secretary

U.S. Geological Survey
Suzette M. Kimball, Acting Director

U.S. Geological Survey, Reston, Virginia: 2014
First release: December 2014

Suggested citation:
Hudnut, K.W., Brocher, T.M., Prentice, C.S., Boatwright, J., Brooks, B.A., Aagaard, B.T., Blair, J.L., Fletcher, J.B., Erdem, J.E., Wicks, C.W., Murray, J.R., Pollitz, F.F., Langbein, J., Svarc, J., Schwartz, D.P., Ponti, D.J., Hecker, S., DeLong, S., Rosa, C., Jones, B., Lamb, R., Rosinski, A., McCrink, T.P., Dawson, T.E., Seitz, G., Rubin, R.S., Glennie, C., Hauser, D., Ericksen, T., Mardock, D., Hoirup, D.F., and Bray, J.D., 2014, Key recovery factors for the August 24, 2014, South Napa earthquake: U.S. Geological Survey Open-File Report 2014–1249, 51 p., *http://dx.doi.org/10.3133/ofr20141249.*

ISSN 2331-1258 (online)

Executive Summary

Through discussions between the Federal Emergency Management Agency (FEMA) and the U.S. Geological Survey (USGS) following the South Napa earthquake, it was determined that several key decision points would be faced by FEMA for which additional information should be sought and provided by USGS and its partners. This report addresses the four tasks that were agreed to. These tasks are (1) assessment of ongoing fault movement (called afterslip) especially in the Browns Valley residential neighborhood, (2) assessment of the shaking pattern in the downtown area of the City of Napa, (3) improvement of information on the fault hazards posed by the West Napa Fault System (record of past earthquakes and slip rate, for example), and (4) imagery acquisition and data processing to provide overall geospatial information support to FEMA.

Actionable Information on Key Recovery Factors, as Identified by FEMA:

1. Afterslip in the Browns Valley neighborhood and surrounding area (see accompanying map on pg. v)
    - The southern part of the main strand of the West Napa Fault within Browns Valley, from south of Leaning Oak Drive up to Partrick Road (A to B on map), that is shown in yellow on the accompanying map, is forecast to experience continued afterslip of an amount that is estimated in detail in this report.
    - The northern part of the main strand of the West Napa Fault within Browns Valley, north of Partrick Road (C to D on map), has experienced no significant afterslip; low afterslip hazard exists on this part of the main strand of the West Napa Fault System.
    - The newly named "eastern strand" of the West Napa Fault System (E to F on map) has experienced no afterslip; low afterslip hazard exists on this eastern strand.
    - Other fault strands shown in green on the accompanying map also have low afterslip hazard.
    - Although the forecasted afterslip in the southern part of the Browns Valley neighborhood (A to B in yellow on map) from Leaning Oak Drive to Partrick Road poses an ongoing hazard to structures, the amount of afterslip is not so great as to pose a highly severe ongoing hazard. The afterslip and associated hazard decreases exponentially with time, posing a moderate hazard.
    - Afterslip along the southern part of the main strand of the fault from Cuttings Wharf Road to Henry Road (shown in fig. 19) poses an ongoing hazard to critical lifelines; this report forecasts an additional 5 to as much as 15 centimeters of afterslip within the next 3 years, particularly along the main fault strand between South Avenue (NSAV in fig. 14) and Highway 12 (shown in fig. 19).
    - A sizable aftershock could lead to significantly increased afterslip, possibly including areas not currently experiencing afterslip.
    - Earthquakes such as an $M7$ scenario event on the Hayward Fault could produce afterslip with much greater severity than experienced in the South Napa earthquake. Afterslip has not previously been considered sufficiently during prior planning exercises, but based on South Napa and other cases, clearly it should be built into future exercises such as the upcoming HayWired scenario.∗
2. Shaking patterns and amplification effects in the City of Napa downtown area
    - Shaking-related damage was distributed uniformly, and not clustered, within the downtown area.
    - Damage levels observed were consistent with recorded substantial shaking loads.
    - Chimney-related damage contributed significantly to overall damage.

∗*http://www.usgs.gov/natural_hazards/safrr/projects/haywired.asp.*

- Shaking from aftershocks recorded by portable seismometers does not identify spatially variable amplification in downtown Napa.
- There is no seismological justification for relocating rather than repairing in place, given that the valley floor is equally susceptible to basin-related amplification effects. Basin-edge effects were noted but are subtle. Within the downtown area, it would be difficult to relocate structures to a less susceptible location with any certainty, based on the analysis of available seismic data shown in this report.
- Regional shaking hazard from aftershocks is still an important consideration.

3. Fault hazards associated with the West Napa Fault System
    - Prior to the South Napa earthquake, the West Napa Fault System had been recognized and mapped, yet the ruptures that had the most fault slip (main strand from A to B and C to D on accompanying map, as well as eastern strand from E to F on map) were on previously unmapped strands. The California Geological Survey is remapping fault zones, according to their role in the Alquist-Priolo Earthquake Fault Zoning Act (California Code of Regulations, Section 3603(f)), along these and other strands of the West Napa Fault System using imagery, some of which is being actively provided by this project to support and help guide their mapping.
    - Even though some fault strands that cross residential areas have only a low ongoing afterslip hazard, these same fault strands that are shown in both green and yellow on the accompanying map are all nevertheless potentially susceptible to future earthquake rupture hazard. That hazard is greater than had been recognized prior to the South Napa earthquake; a thorough reevaluation is under way at this time.
    - Excavations that were already in progress, as well as new excavations, are in the process of being examined as part of this project, with the aim of gaining new information on long-term fault hazards that support future decisions on appropriate land use and development.
4. Imagery
    - Rapid aerial reconnaissance provides an overview of the fault rupture and impacts to critical lifeline infrastructure along the fault rupture. For the South Napa earthquake, prior planning and exercises (conducted by California Highway Patrol [CHP], the California Earthquake Clearinghouse, CGS, California Department of Transportation, USGS, and others) expedited rapid aerial reconnaissance and proved vital to coordination that resulted in the timely prioritization and acquisition of aerial imagery (especially the air photos acquired by CHP and USGS on August 25, 2014).
    - For the South Napa earthquake, rapid acquisition of aerial photos and LiDAR (especially the imagery collected on September 9, 2014), as well as satellite and airborne imagery from a variety of sensors and platforms, was well supported and coordinated; that imagery is available primarily through USGS Earth Resources Observation and Science (EROS) Hazards Data Distribution System (HDDS).

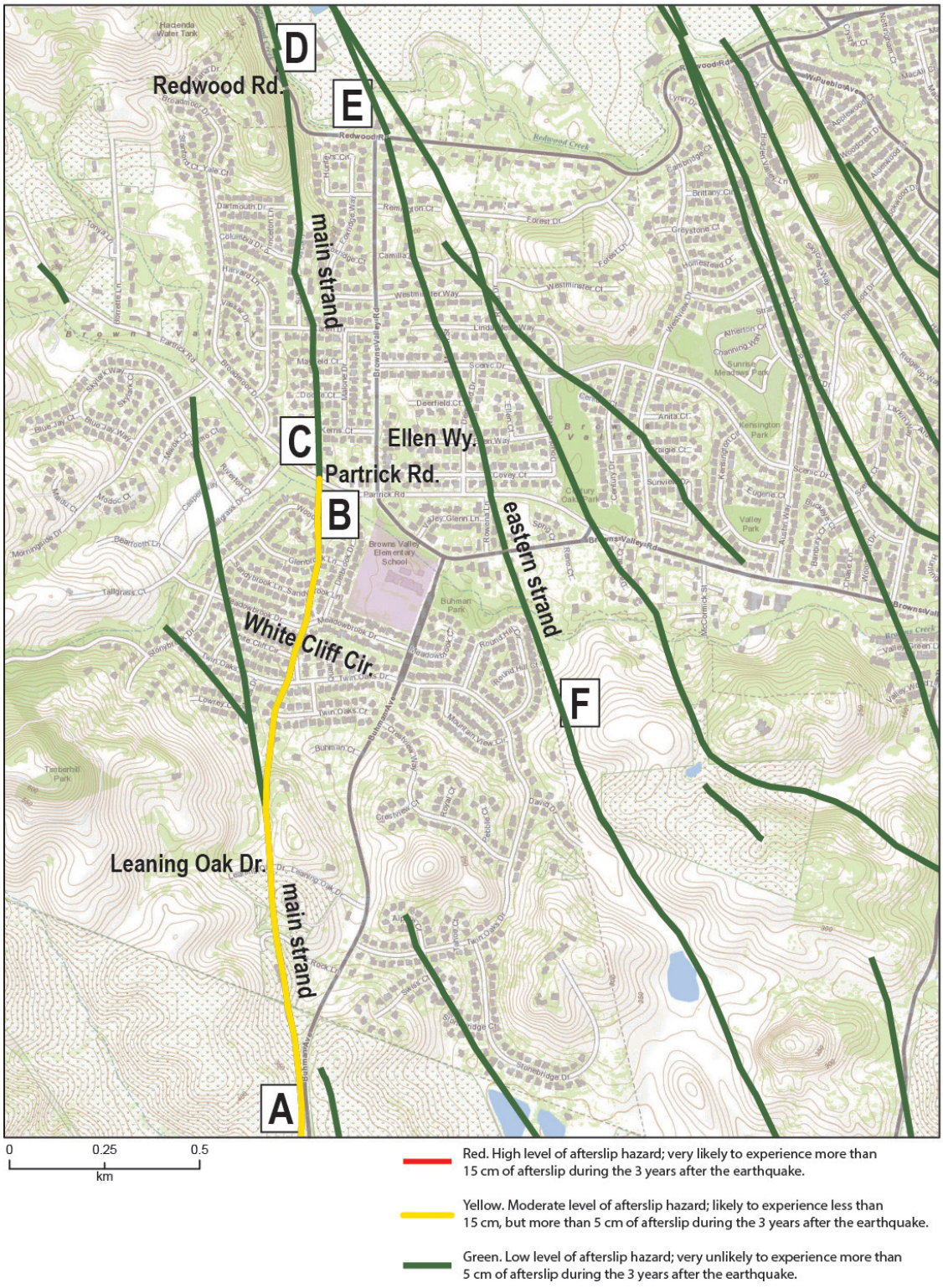

Afterslip hazard map of the Browns Valley neighborhood and surrounding area. A detailed map explanation is presented on the following page.

Caption for map on previous page:

Levels of Afterslip Hazard for the Browns Valley Neighborhood, City of Napa, California:

All fault traces shown on this map face potential future earthquake fault surface rupture hazard and other earthquake-related hazards such as shaking, liquefaction, and landslides; these hazards are treated separately in other publications and maps from CGS and USGS (with preliminary updates provided in this report).

For all levels of afterslip hazard, the afterslip amount that is measured 90 days after the earthquake can be expected to as much as double by 10 years after the earthquake (less than double is also possible).

Red Fault Trace—High level of afterslip hazard; very likely to experience more than 15 cm of afterslip during the 3 years after the earthquake. (Red is intentionally included, even though none is indicated on this map.)

Yellow Fault Trace—Moderate level of afterslip hazard; likely to experience less than 15 cm, but more than 5 cm, of afterslip during the 3 years after the earthquake. (Additional afterslip accumulation is likely to gradually accumulate an additional 5 cm during the 10 years after the earthquake and an additional 5 cm 30 years after the earthquake.)

Green Fault Trace—Low level of afterslip hazard; very unlikely to experience more than 5 cm of afterslip during the 3 years after the earthquake. (Faults that experienced <10 cm of coseismic offset and <5 cm of afterslip within the 3 months after the earthquake are included in this category. Some faults or lineaments shown as green had no measurable coseismic slip or afterslip associated with the August 24, 2014, earthquake. Faults and lineaments of several categories are shown for completeness. Some are previously mapped strands (U.S. Geological Survey and California Geological Survey, 2006); others represent preliminary mapping based on a combination of imagery interpretation and field mapping that has taken place since the August 24, 2014, earthquake. All of the faults and/or imagery lineaments shown as heavy green lines on this map may be considered to have a low level of afterslip hazard. Subsequent ongoing mapping, that is, work still in progress, may reveal that certain lineaments shown here are not actually faults.)

Map orientation: North direction is toward top of map.

Preface

Subjects of significance to FEMA assistance programs, for which the U.S. Geological Survey is able to provide useful information, were identified as the basis for an agreement for specialized work on the South Napa earthquake (*M*6.0). These subjects include the following: (1) fault afterslip, especially ongoing (yet diminishing) afterslip in the Browns Valley residential neighborhood; (2) shaking and correlation to damage such as red- and yellow-tagged structures, especially in the downtown Napa area; (3) seismic hazards of the West Napa Fault System, especially in residential areas; and (4) geospatial analysis and imagery support (such as post-processing of LiDAR and other imagery that has already been acquired). In this report, USGS provides information on these subjects. It is mutually understood by FEMA and USGS that the contents of this report are preliminary in nature and provided as best available information on a necessarily short time scale to be of most use to FEMA for making decisions as soon as possible.

Acknowledgments

We thank the many landowners and property managers along the entire length of the fault rupture and other adjacent areas of ground deformation and disturbance, and in Browns Valley and throughout Napa, for allowing us access to perform the wide variety of field work necessary to produce this report. We especially thank Julie Arbuckle, Gustavo Avina, Michael Beaulac, Zach Berkowitz, Armando Ceja, Pablo Ceja, Robert DeLeuze, Rob and Kristan Forloine, David Graves, Chris Gurney, Toby Hallkovich, Maxine Jacobs, Steven Moulds, Theo Perez, Tony Trouchard, Al Wagner, Dana Zaccone, and Debby Zygielbaum. For providing the updated red and yellow tag data files used in figures 1, 2, and 5, we thank Katy Wallis from the City of Napa. For helicopter support of the initial aerial reconnaissance and aerial photography on August 24–25, 2014, we thank Michael Sedam and the California Highway Patrol at the Napa County Airport as well as Derek Kantar of Caltrans and the California Air Coordination Group. We also thank Martin Pehl, Airport Manager, County of Napa, for allowing access to their active runways to examine and map the fault rupture. We thank the California Integrated Seismic Network and Plate Boundary Observatory for use of their data. We also thank Scott Hensley, Andrea Donnellan, and the entire UAVSAR project team at NASA's Jet Propulsion Laboratory (JPL) for providing browse product images (such as the example shown in fig. 17). We thank the ARIA group at Caltech and JPL for imagery we used extensively to help guide the surface rupture mapping and assess afterslip. We also thank the reviewers of this report: Jeff Rowbotham (FEMA), Emile Wong (FEMA), Sam Ronveaux (FEMA), Michael Hornick (FEMA), Dale Cox (USGS), Tom Holzer (USGS), Katherine Kendrick (USGS), Mike Diggles (USGS), Carolyn Donlin (USGS), and Jessica Dyke (USGS). Finally, we especially thank James Lienkaemper (USGS) for his input on earlier drafts of this report and for allowing inclusion of figures that show his alinement array results.

Contents

Figures

Tables

Conversion Factors

International System of Units to Inch/Pound

Multiply	By	To obtain
	Length	
centimeter (cm)	0.3937	inch (in.)
millimeter (mm)	0.03937	inch (in.)
meter (m)	3.281	foot (ft)
kilometer (km)	0.6214	mile (mi)
kilometer (km)	0.5400	mile, nautical (nmi)
meter (m)	1.094	yard (yd)
	Area	
square meter (m^2)	0.0002471	acre
hectare (ha)	2.471	acre
square hectometer (hm^2)	2.471	acre
square kilometer (km^2)	247.1	acre
square centimeter (cm^2)	0.001076	square foot (ft^2)
square meter (m^2)	10.76	square foot (ft^2)
square centimeter (cm^2)	0.1550	square inch (in^2)
square hectometer (hm^2)	0.003861	section (640 acres or 1 square mile)
hectare (ha)	0.003861	square mile (mi^2)
square kilometer (km^2)	0.3861	square mile (mi^2)

Datum

Unless specifically noted in the associated metadata that accompanies the wide array of imagery contained in this report:

- Vertical coordinate information is referenced to the North American Vertical Datum of 1988 (NAVD 88).
- Horizontal coordinate information is referenced to the North American Datum of 1983 (NAD 83).
- Altitude, as used in this report, refers to distance above the vertical datum.

Abbreviations

CalOES	California Office of Emergency Services
CGS	California Geological Survey
CHP	California Highway Patrol
EO	Electro-Optical
EROS	Earth Resources Observation and Science
FEMA	Federal Emergency Management Agency

GPS	Global Positioning System
HDDS	Hazards Data Distribution System
InSAR	Interferometric Synthetic Aperture Radar
LiDAR	Light Detection And Ranging
SAR	Synthetic Aperture Radar
UAVSAR	Uninhabited Aerial Vehicle Synthetic Aperture Radar
USGS	U.S. Geological Survey
WNFS	West Napa Fault System

Key Recovery Factors for the August 24, 2014, South Napa Earthquake

By Kenneth W. Hudnut,[1] Thomas M. Brocher,[1] Carol S. Prentice,[1] John Boatwright,[1] Benjamin A. Brooks,[1] Brad T. Aagaard,[1] J. Luke Blair,[1] Joe B. Fletcher,[1] Jemile E. Erdem,[1] Charles W. Wicks,[1] Jessica R. Murray,[1] Fred F. Pollitz,[1] John Langbein,[1] Jerry Svarc,[1] David P. Schwartz,[1] Daniel J. Ponti,[1] Suzanne Hecker,[1] Stephen DeLong,[1] Carla Rosa,[1] Brenda Jones,[1] Rynn Lamb,[1] Anne M. Rosinski, [2] Timothy P. McCrink,[2] Timothy E. Dawson,[2] Gordon Seitz,[2] Ron S. Rubin,[2] Craig Glennie,[3] Darren Hauser,[3] Todd Ericksen,[4] Dan Mardock,[5] Don F. Hoirup,[5] and Jonathan D. Bray[6]

Abstract

The U.S. Geological Survey (USGS) and partners analyzed specialized information from the *M*6.0 South Napa earthquake on selected topics relevant to FEMA (Federal Emergency Management Agency) programs, and, in particular, those programs associated with response and recovery. This report for FEMA is a summary of our findings. This report provides fault afterslip, shaking and damage in the City of Napa downtown area, and fault hazards of the West Napa Fault System, as well as associated geospatial information and imagery. Initially, the fault afterslip was rapid and extended into at least the southern part of the Browns Valley neighborhood. USGS forecasts the afterslip for homes potentially impacted by future afterslip. The shaking recorded in the downtown City of Napa is consistent with the observed damage, and the pattern of damage is relatively uniform. There is no evidence for the shaking being strongly amplified in any particular pockets of the downtown area. All parts of the Napa downtown area are (within a factor of about three) nearly equally vulnerable to future shaking amplification. The fault hazard of the West Napa Fault System is still being re-evaluated at this time. Faults that broke in residential areas and caused damage to many homes during this earthquake, in some but not all cases, had not previously been mapped. Fault strands that had been mapped prior to this earthquake were not known to be highly hazardous, but that is being re-evaluated. The State is currently remapping the West Napa Fault System, and that work is in progress and supported by some of the imagery acquisitions that have been completed, are being planned or are in progress.

[1]U.S. Geological Survey
[2]California Geological Survey
[3]University of Houston
[4]University of Hawai‘i at Manoa
[5]California Department of Water Resources
[6]University of California, Berkeley

Introduction

The August 24, 2014, South Napa earthquake (*M*6.0) produced significant damage resulting from shaking, fault rupture, fault afterslip, and ground deformation. These effects are described in initial reports already published by Geotechnical Extreme Events Reconnaissance (GEER[7]) and Earthquake Engineering Research Institute (EERI[8]). Work by USGS and partners over the 3 months since the earthquake has encompassed many aspects, several of which are significant for FEMA programs. These aspects are as follows: (1) fault afterslip, especially ongoing (yet diminishing) afterslip in the Browns Valley neighborhood; (2) shaking and correlation to damage, such as red- and yellow-tagged structures, especially in the downtown Napa area; (3) fault hazards of the West Napa Fault System, especially in residential areas; and (4) geospatial data and imagery support (such as post-processing and analysis). This report focuses on these particular aspects and extracts information from prior reports and ongoing work to provide FEMA with information that is directly relevant to their programs. It is mutually understood by FEMA and USGS that the contents of this report are preliminary in nature and provided as best available information on a necessarily short time frame.

Analysis of Ground-Motion in the City of Napa

We compiled and analyzed a variety of observations to assess the spatial variability of ground motion within the City of Napa for the August 24, 2014, earthquake and its aftershocks. The distribution of red- and yellow-tagged structures suggests that the deeper geologic structure, namely, a sedimentary basin underneath the City of Napa, contributed to stronger shaking in downtown Napa. Seismic instruments deployed to record aftershocks in the downtown area indicate that the ground motions at all the stations in downtown Napa are similar in amplitude across a wide range of frequencies. Thus, we do not find any evidence that the mainshock motions recorded at USGS permanent seismic station N016 (location shown on figure 1) are significantly different than the motions for other areas within downtown Napa. That is, the ground motion recorded by station N016 is representative of the ground motions that damaged a wide area of downtown Napa.

The Distribution of Red and Yellow Tags in the City of Napa

The South Napa earthquake strongly shook the City of Napa, damaging both residential and commercial buildings from Browns Valley through the historic downtown. The damage to wood-frame houses largely occurred as broken and cracked chimneys, although a number of houses were shifted on their foundations or suffered racking or failure of cripple walls (Earthquake Engineering Research Institute, 2014). In the downtown area, many masonry buildings, both unreinforced and retrofitted, were damaged, including the part of the Napa Courthouse built in 1870 (Earthquake Engineering Research Institute, 2014).

The City of Napa, with the assistance of structural engineers who volunteered from many areas across California, tagged and retagged damaged structures throughout the city. The tagging data was provided to the USGS by Katy Wallis, GIS Coordinator for the City of Napa; these data provide a

[7] *http://www.geerassociation.org/GEER_Post%20EQ%20Reports/SouthNapa_2014/index.html.*
[8] *https://www.eeri.org/2014/08/m6-0-south-napa-california-earthquake-california-earthquake-clearinghouse/.*

complete municipal report of prohibited (red tags) or restricted (yellow tags) access to earthquake-damaged structures.

The dataset provided on November 5, 2014, contains 165 red tags and 1,707 yellow tags. Of these, 193 tags were multiple tags for the same buildings, corresponding to multiple inspections. Twenty-four tags restricted access to undamaged structures owing to damage of adjacent or nearby structures. We removed these tags from the dataset to avoid duplicate counting of damaged buildings. Thus each tag in the dataset used in the analysis corresponds to a single damaged or unsafe building.

The red and yellow tags extend across the City of Napa, from Browns Valley to the west into the hills to the east of the Napa River (fig. 1). The densest concentration of red and yellow tags occurs in a 2.5- x 1.5-km kidney-shaped area that is bounded on the east by the Napa River and extends 1.5 km northwest and 2 km southwest of the downtown area. Herein, we refer to this area as the "Napa damage zone." The red and yellow tags appear approximately uniform within this zone, although there is a cluster of red tags in the historic downtown area in the blocks between 1st and 3rd Streets, and Main and Coombs Streets.

Although there are clusters of yellow tags in the northwest, north, and northeast sections of the city, the tags in these areas are generally less dense and less extensive than the tags in the Napa damage zone. There are very few tags in the eastern section of Napa. More critically, there are relatively few tags to the west of the damage zone, closer to the earthquake fault but still within the Napa Valley, where one might have expected the ground motion to be stronger than in the downtown area.

Figure 1 shows the red and yellow tags relative to the surficial mapped geology (Witter and others, 2006). There are several alluvial units mapped within the Napa Valley. The youngest unit, Qhty (Late Holocene stream terrace deposits), follows the Napa River and contains relatively few tagged structures, although it includes the eastern edge of the Napa damage zone. The next youngest units, Qhf (Holocene alluvial fan deposits) and Qhf2 (Holocene intermediate alluvial fan deposits), underlie most of the City of Napa and contain most of the tagged structures. An older unit, Qpf2 (Pleistocene older alluvial fan deposits), lies north of the city and contains few tagged structures. The distribution of tagged structures does not exhibit a strong correlation with the mapped geology (which corresponds to the near-surface geologic structure).

The red- and yellow-tagged structures are plotted over the depth to bedrock in the USGS Bay Area 3-D Seismic Velocity Model (Aagaard and others, 2010) in figure 2. The seismic velocity model contains a sedimentary basin that underlies the City of Napa. The deepest part of the basin sits south of the downtown area, but a shallow arm of the basin extends 9 km to the northwest. The distribution of tagged structures correlates reasonably well with the edges of the sedimentary basin, in particular, along the western and eastern edges of the Napa damage zone, and throughout the shallow northern reach of the basin. This correlation diminishes to the southeast, where the basin extends a few kilometers into a region with fewer structures and few red- and yellow-tagged structures. These correlations are consistent with numerous studies that have demonstrated amplification due to converted phases at edges of sedimentary basins (Vidale and Helmberger, 1988; Graves and others, 1998).

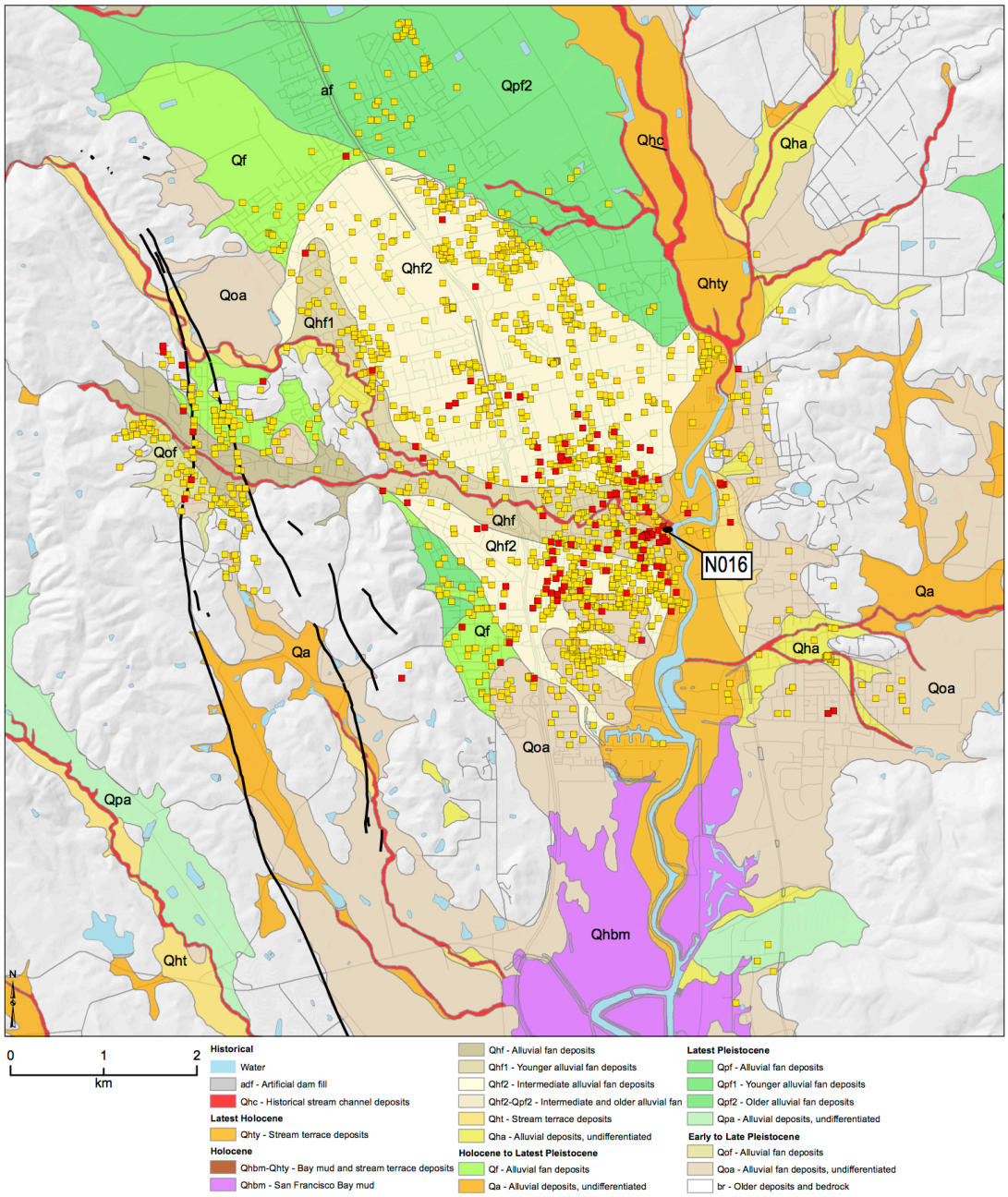

Figure 1. Locations of red- and yellow-tagged structures overlain on Witter and others' (2006) geologic map. A solid black oval shows location of station N016, which is in downtown Napa, Calif.

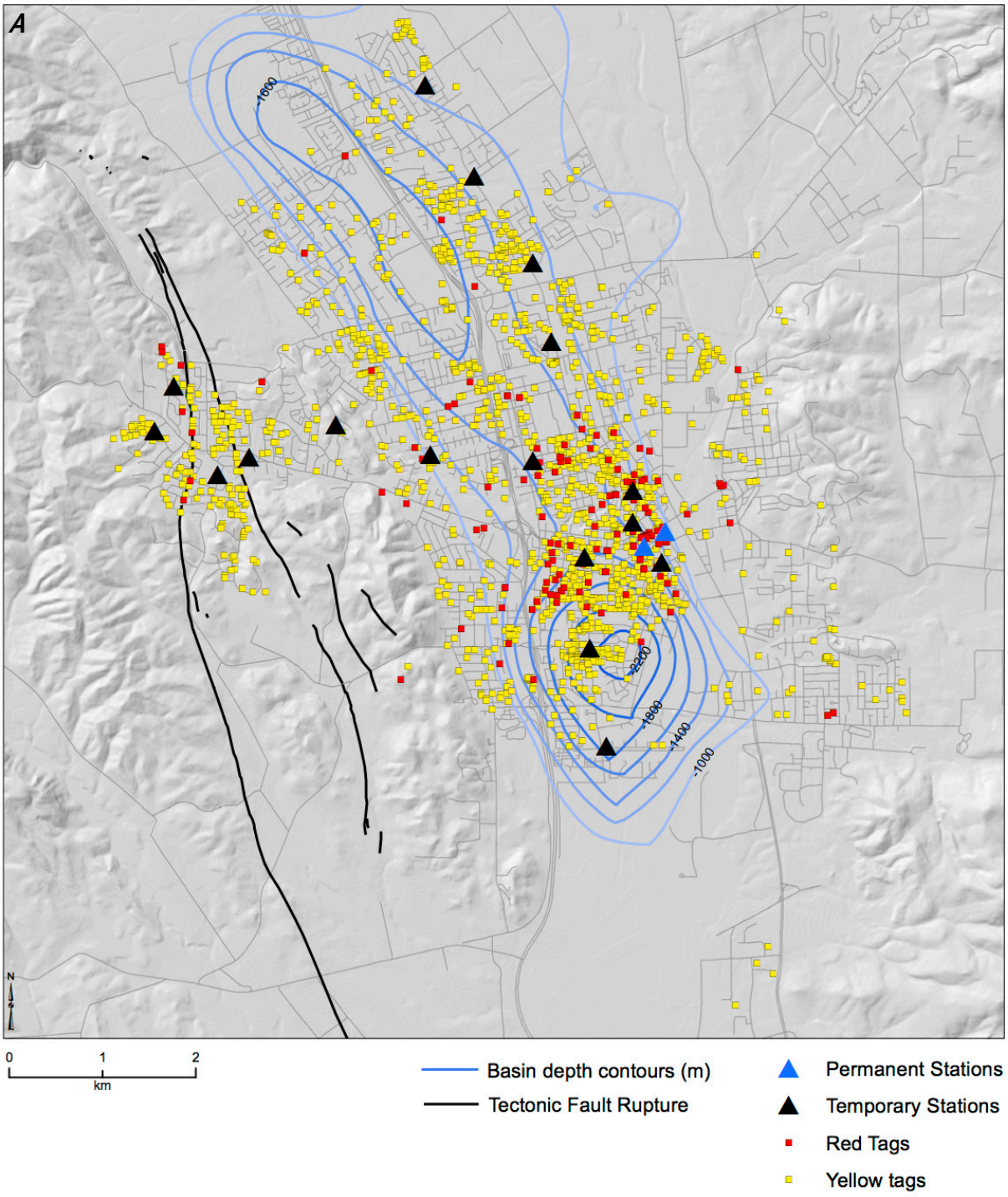

Figure 2*A* caption shown on p. 7.

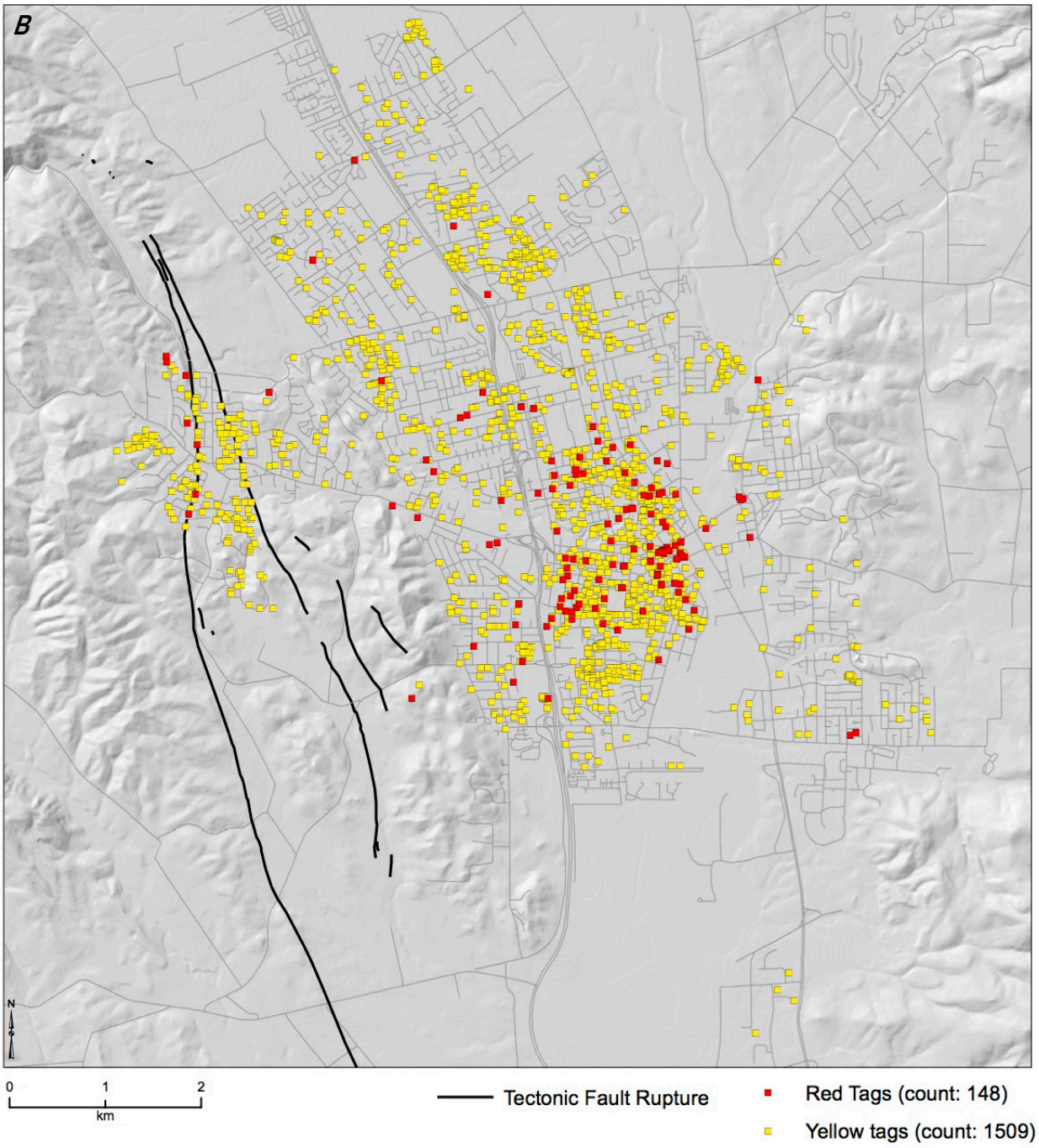

Figure 2*B* caption shown on p. 7.

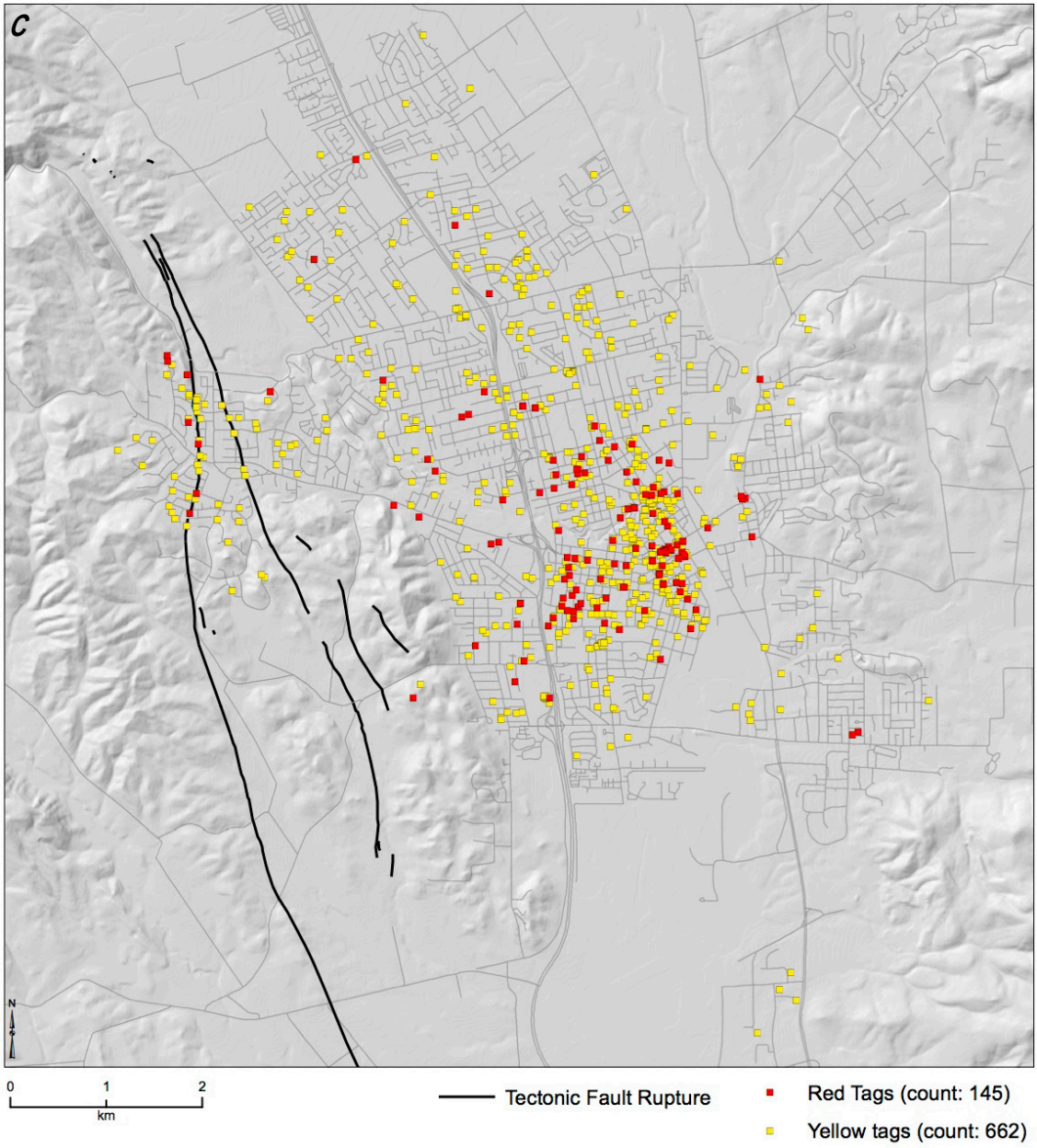

Figure 2. Maps showing red- and yellow-tagged structures and faults in Napa, Calif. *A*, Red- and yellow-tagged structures with blue lines showing thickness of the Napa Basin, in meters, from the USGS Bay Area 3-D Seismic Velocity Model (Aagaard and others, 2010). The inferred basin is deeper (2,500 m) to the south of downtown Napa than to the north (1,500 m). *B*, Locations of red- and yellow-tagged structures, showing all red- and yellow-tagged structures (that is, prior to the removal of structures damaged by chimneys cracking or falling). *C*, Locations of red- and yellow-tagged structures. Tags associated with chimney-related damage have been removed, revealing damage other than that related to chimneys. The trend along the fault rupture through Browns Valley becomes clearer, with chimney damage data points removed. Notes in the database indicate that these structures were damaged by surface faulting and afterslip, as well as shaking. Note the significantly decreased counts of red- and yellow-tagged structures.

Ground Motions Recorded in the Downtown Area

The South Napa mainshock was recorded by a single instrument in downtown Napa, station N016, operated by USGS and located at a restaurant on 2nd and Main Streets. The 3-component acceleration and velocity waveforms are plotted in figure 3. The strongest ground motions, peak ground acceleration (PGA) = 61 percent gravity (g) and peak ground velocity (PGV) = 47 cm/s, occurred on the northern horizontal component.[9]

The waveforms in figure 3 exhibit two important characteristics. First, the duration of the strongest accelerations, the S-wave pulse, is relatively short, lasting only about 2 s. This short duration is a result of the northward rupture directivity in the earthquake (Boatwright, 2014). Second, the velocity and acceleration waveforms exhibit large amplitude motions at periods from 1 to 3 s that persist for 10 s after the initial S-wave arrival. This motion is likely derived from the sedimentary basin underlying the City of Napa, depicted in figure 2*A*.

Figure 4 shows the 5 percent damped acceleration response spectra for the three components of the N016 recording. The response spectrum for the north component exceeds 1.2 g from 0.3 to 0.6 s, consistent with high enough levels of ground motions in the period band necessary to cause significant damage to buildings of 3 to 6 stories (Housner, 1959).

The U.S. Geological Survey deployed 16 seismic instruments in Napa for several weeks following the South Napa earthquake. Four of these instruments were sited in the downtown area near station N016. Figure 5 identifies the station locations together with the distribution of red- and yellow-tagged structures.

We determine the relative amplification of these sites by applying the analysis technique of Boatwright and others (1991). The temporary stations recorded four aftershocks ranging in magnitude from *M*2.6 to *M*3.2. The hypocentral distances to the stations are compiled in table 1.

Table 1. Aftershock recordings of the South Napa earthquake.

Date	Origin	Magnitude	N016	N020	SN09	SN10	SN11
	Time		km	km	km	km	km
8/31/2014	08:56:21	3.2	12.6	12.2	12.6	12.8	12.4
9/3/2014	10:18:51	2.6	12.7	12.3	12.7	12.9	12.5
9/4/2014	10:56:23	2.9	no record	16.9	17.2	17.5	16.9
9/21/2014	20:17:54	2.6	12.7	12.3	12.5	12.4	12.8

[9]N016 (USGS NCSN) data may be downloaded from *http://strongmotioncenter.org/cgi-bin/CESMD/iqr_dist_DM2.pl?iqrID=AmericanCanyon_24Aug2014_72282711*.

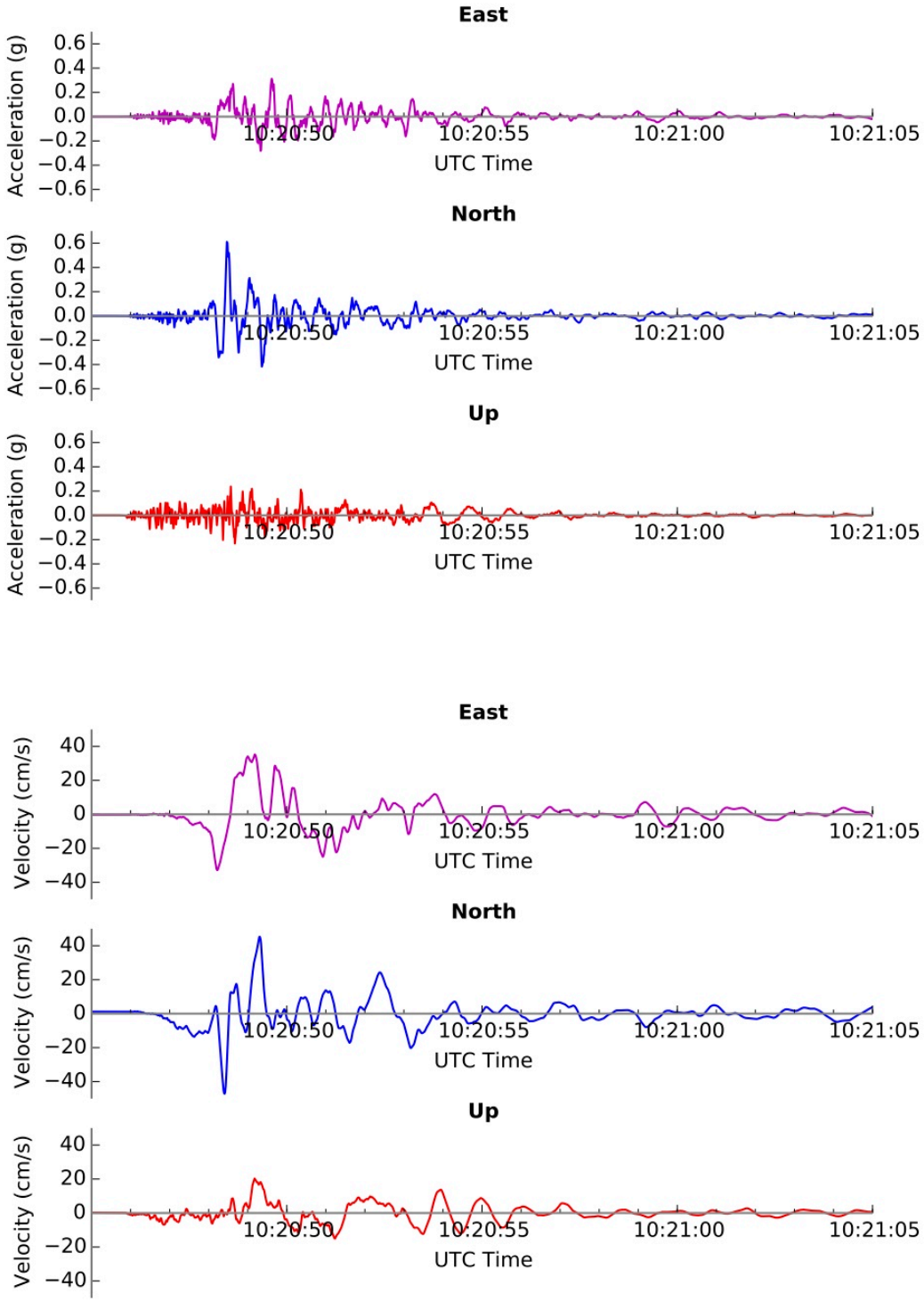

Figure 3. Graph showing acceleration and velocity waveforms from the mainshock of the August 24, 2014, South Napa earthquake for station N016.

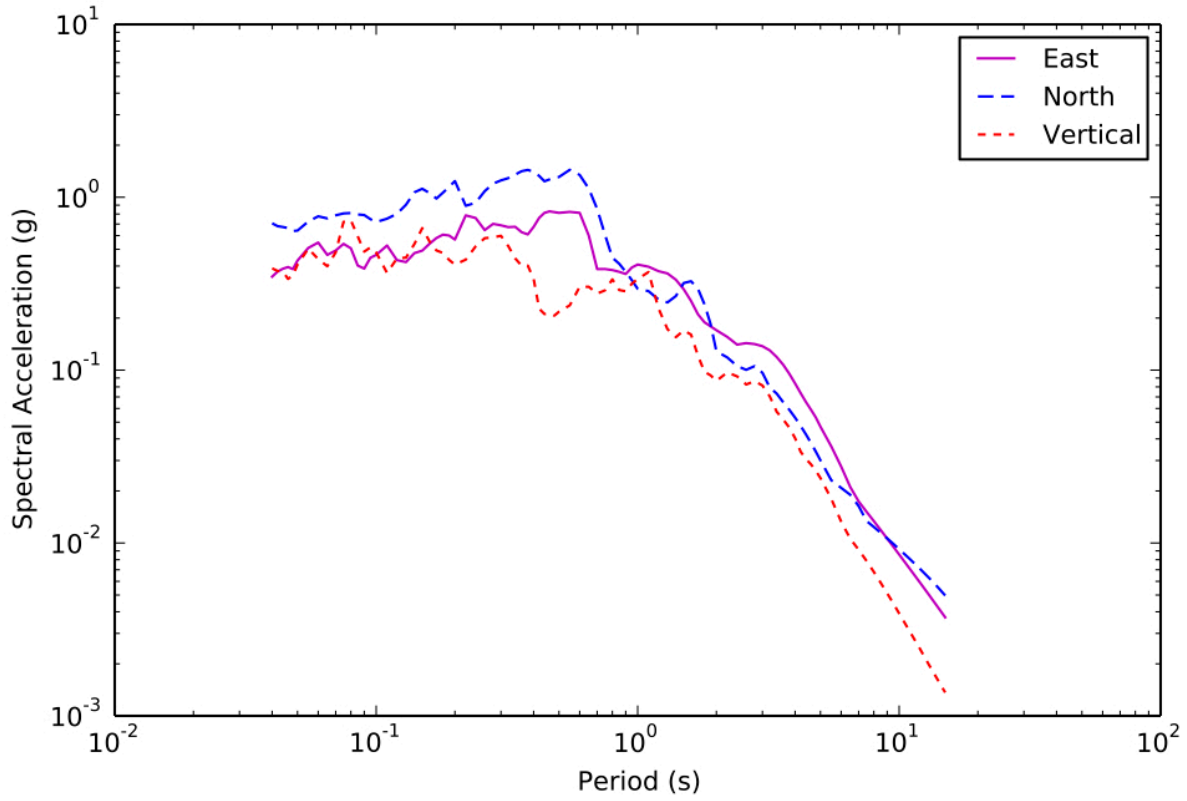

Figure 4. Graph showing acceleration response spectra for station N016 located near Napa, Calif.

The seismic stations have different noise characteristics as a result of deploying two types of instruments. Stations SN09, SN10, and SN11 were equipped with broadband seismographs, while stations N016 and N020 were equipped with NetQuake accelerographs. The NetQuake accelerographs are relatively noisy at long periods; consequently, we down-weight the spectral amplitudes below 0.4 Hz from these instruments for the three smallest aftershocks to minimize the long-period distortion of the relative amplifications.

The analysis can only determine relative, not absolute, amplifications. One station must be used as a reference to normalize the amplifications. We use station SN09 as a reference because it is located in the middle of the set of stations and it is a broadband accelerograph with a lower noise floor.

We find little variation in ground motions with amplification relative to station SN09 close to 1.0 for periods between 0.05 s (20 Hz) and 1.0 s as illustrated in figure 6. At periods less than about 0.3 s (3 Hz), the amplitudes at stations N016 and N020 are 30 to 50 percent lower than the other stations at some periods. This reduced amplification could result from stronger attenuation in recently deposited (Holocene) alluvium. Thus, based on the limited variability in amplitude across the instruments recording aftershocks in the downtown area, we conclude that the mainshock ground motions were approximately uniform across the downtown area (although two- to three-fold variation in shaking is shown in figure 6).

Finally, to give a comprehensive overview of the regional shaking, we include figure 7, which shows a compilation of all available peak ground acceleration data. Earlier maps such as the USGS ShakeMap have shown a variety of modeled or otherwise interpolated values and approximations of regional shaking intensities, but the map in figure 7 differs because it shows only actual recorded values.

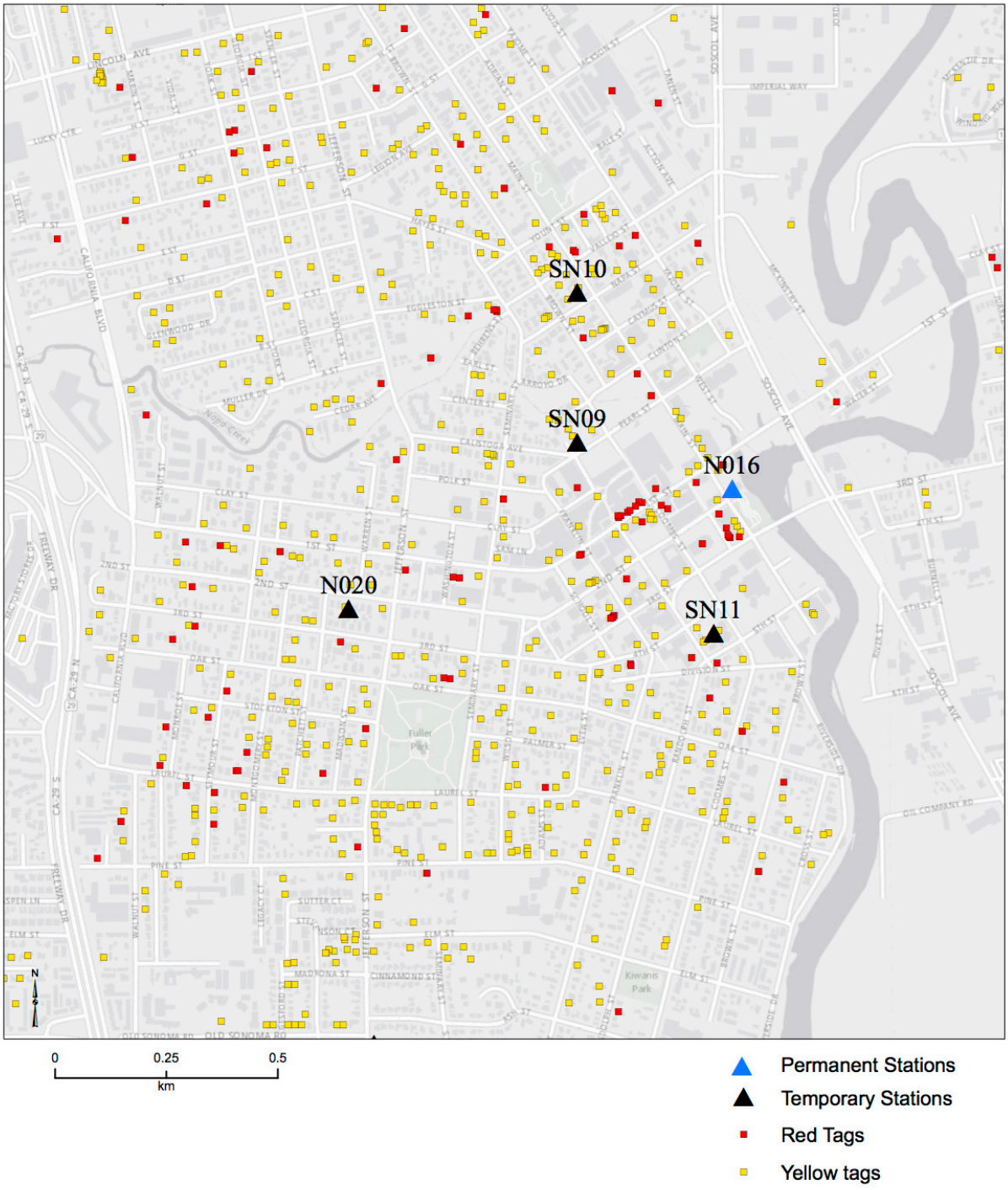

Figure 5. Map showing red- and yellow-tagged structures as well as seismic stations in downtown Napa, Calif.

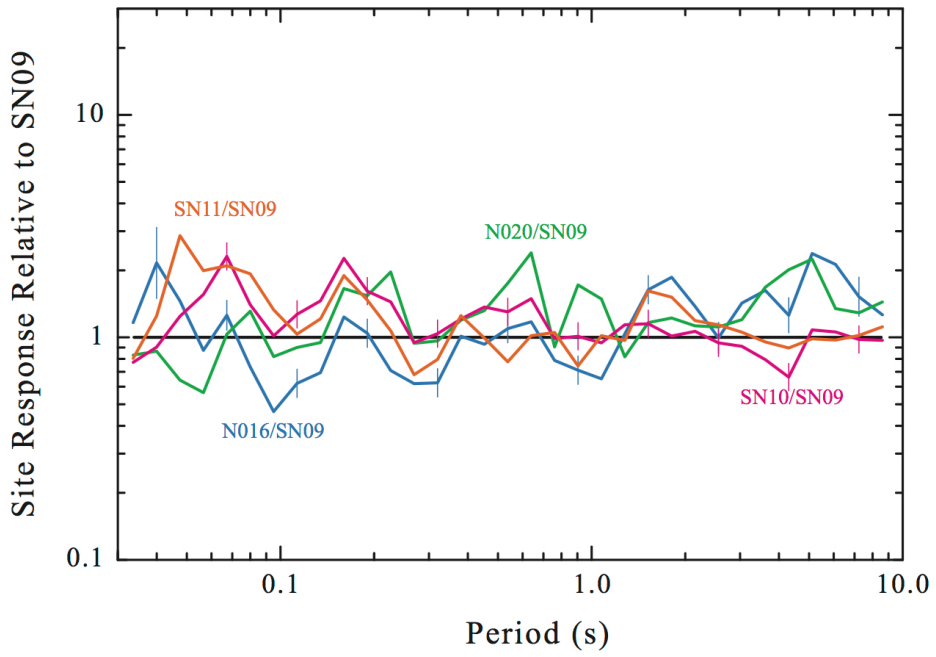

Figure 6. Graph showing amplification measured at stations N016, N020, SN10, and SN11, relative to that measured at station SN09, as a function of period for the August 24, 2014, South Napa earthquake.

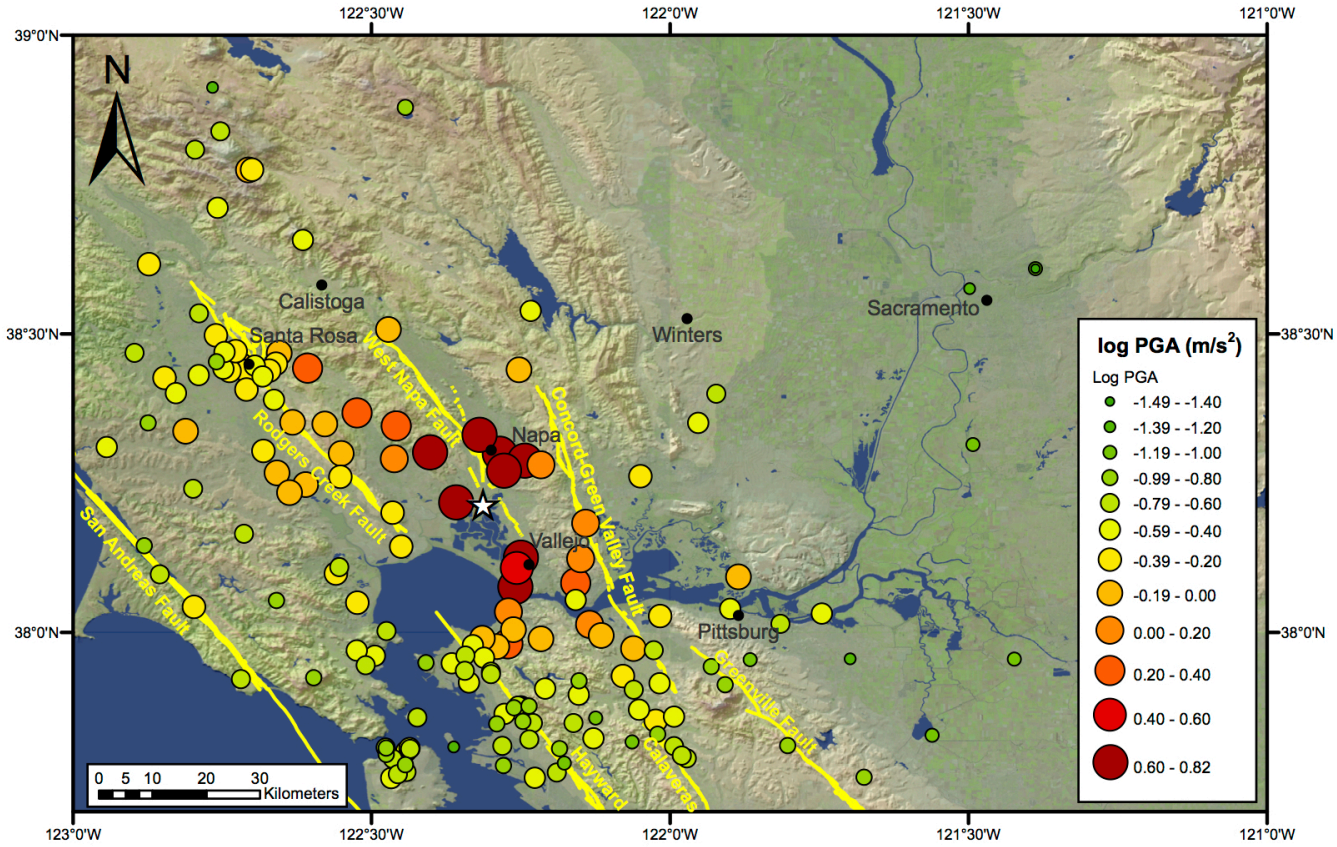

Figure 7. Map showing peak ground acceleration data for the August 24, 2014, South Napa earthquake. Station symbols are colored and scaled by log PGA in m/s^2 and given by scale on right. Earthquake epicenter is indicated by the star.

Analysis of Fault Afterslip

Afterslip Along the Entire Fault Length

Associated with the earthquake, an unusually large amount of fault slip for a *M*6.0 earthquake occurred on strands of the West Napa Fault System. Soon after the earthquake, parts of the fault were continuing to slip. This is a well-known phenomenon called afterslip that has been previously described for many earthquakes, including several well-studied cases in California, for example, the 1979 Imperial Valley, 1987 Superstition Hills, and 2004 Parkfield earthquakes. Afterslip occurs quickly at first, then slows down and is thought to eventually stop long after the earthquake. Data are typically well fit by variants of exponential time-decaying functions. Data collected for prior occurrences of afterslip on California faults have been used to define these time-decay curve functions. To put bounds on the realistic long-term extrapolation errors, other types of curves have also been fit to the data for the South Napa earthquake as part of this report. It is critical to understand not only the best long-term forecast of afterslip, but also the formal uncertainties (the expected unknowns) and epistemic uncertainties (the unexpected unknowns). Several main types of data were used by USGS to estimate the afterslip and forecast it, with special attention given to the Browns Valley residential neighborhood. The data show that the afterslip will continue to increase the amount of fault displacement over the upcoming years on part of the main fault strand. The data also show that other parts of the main fault strand are not experiencing any afterslip. The secondary fault traces that broke during the earthquake in the residential areas of Browns Valley and to the east of it are not experiencing afterslip. So we pay special attention, as well, to identifying all those fault strands that are not considered susceptible to ongoing fault slip in the upcoming years. Those fault sections that are not continuing to slip must, however, still be considered hazardous, and the CGS is remapping the West Napa Fault System concurrently to redefine the Alquist-Priolo Special Fault Studies zones for the region as a result of this earthquake. That is, a house that is located on a trace of the fault zone that experienced coseismic fault slip, but that is not experiencing afterslip (and therefore not expected to experience further slip), may be considered “low” in terms of afterslip hazard only. In this report, we are not attempting to address the other hazard of possible fault slip from another earthquake or afterslip from a future earthquake. Furthermore, a sizable aftershock might lead to increased afterslip, possibly including fault strands that are not currently exhibiting afterslip.

First, we must define types of fault slip: coseismic (fault slip during the earthquake) and postseismic (fault slip after the earthquake). Afterslip is a type of postseismic deformation that usually is confined to the uppermost shallow portion (or, alternatively, the deepest portion) of the fault zone. Postseismic deformation, as recorded by GPS stations farther from the fault zone, may be sensitive to motion on deeper portions of the fault zone. Other effects such as movement of fluids can also contribute to postseismic deformation. In our analysis, we combine several data types and compute slip on the fault at the time of the earthquake and afterwards, and we do this for several reasons that are relevant for Browns Valley. If the shallow slip on the fault beneath Browns Valley will eventually catch up to the deep slip, then it would be useful to know the value for the slip at depth. For this reason, we are interested in the coseismic as well as postseismic slip estimates, and we describe both below.

Three types of data recorded coseismic displacement and/or continued motion of the Earth’s surface in the days and weeks following the South Napa earthquake. These are Global Positioning System (GPS) measurements of east (longitude), north (latitude), and vertical motion; Interferometeric Synthetic Aperture Radar (InSAR) measurements of motion of the ground surface in the direction of the SAR satellite; and alinement array measurements of shallow fault parallel motion.

GPS data were recorded in two ways: (1) using permanently installed stations and (2) using temporary deployments of additional instrumentation during the days and weeks following the earthquake. InSAR scenes were recorded by several satellites on various dates before and after the earthquake. Repeated alinement array measurements were made five to seven times (depending on location) following the earthquake.

Continuously operating GPS site P261, located 11 km from the epicenter and operated by UNAVCO, is the continuously recorded site that is nearest to the earthquake (fig. 8).

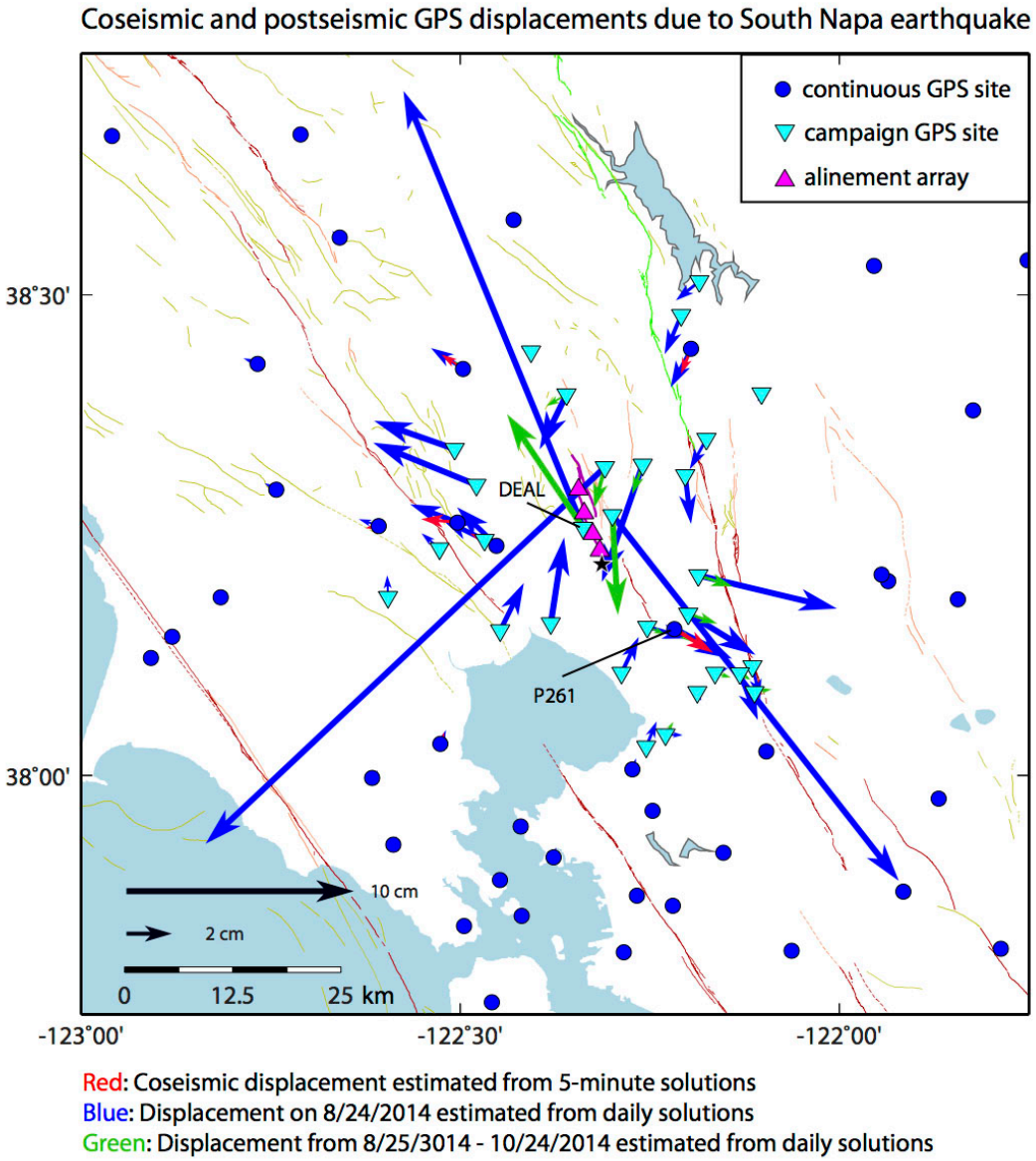

Figure 8. Map showing coseismic and postseismic GPS displacements of the August 24, 2014, South Napa earthquake. Red and blue vectors are both coseismic estimates (using different data and methods). Green vectors are postseismic displacements.

Position solutions calculated at 5-minute intervals from 30 sample per second data (fig. 9) show postseismic motion at this site starting very soon after the earthquake and accumulating an additional ~0.5 cm of displacement over the remaining ~14 hours of August 24, 2014, following the earthquake (UTC time).

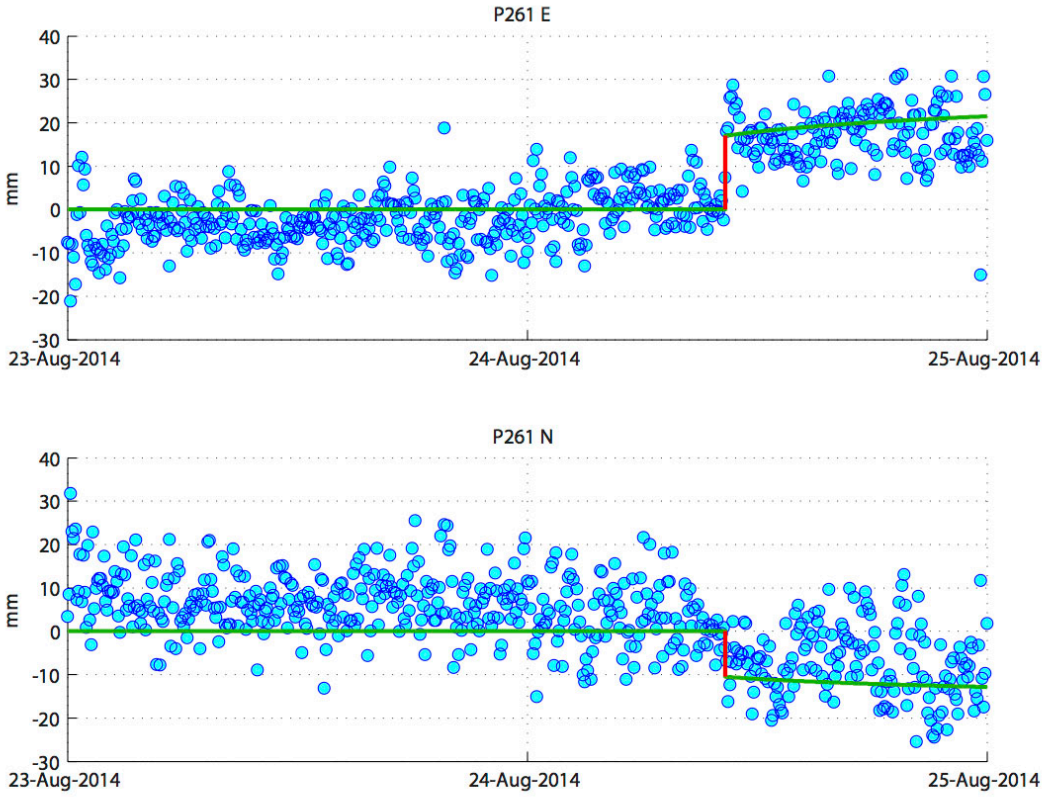

Figure 9. Graph showing GPS results for Plate Boundary Observatory station P261 located near Napa, Calif., with displacement on the y-axis and time on the x-axis. Coseismic offset is in red, and the best fitting postseismic offset is in green.

The P261 PBO site and nine other CGPS sites within ~40 km of the epicenter continued to experience postseismic motion over the weeks following the earthquake, although sites more than ~15 km from the epicenter exhibited very small displacements (fig. 8). The campaign GPS data, while lacking observations for a short time after the event, also exhibit postseismic motion, with station DEAL (5 km from the epicenter, fig. 8) showing the largest signal (fig. 10). Interferograms spanning different portions of the postseismic period, as well as alinement array data, also show clear evidence for postseismic motion in the days to weeks following the earthquake.

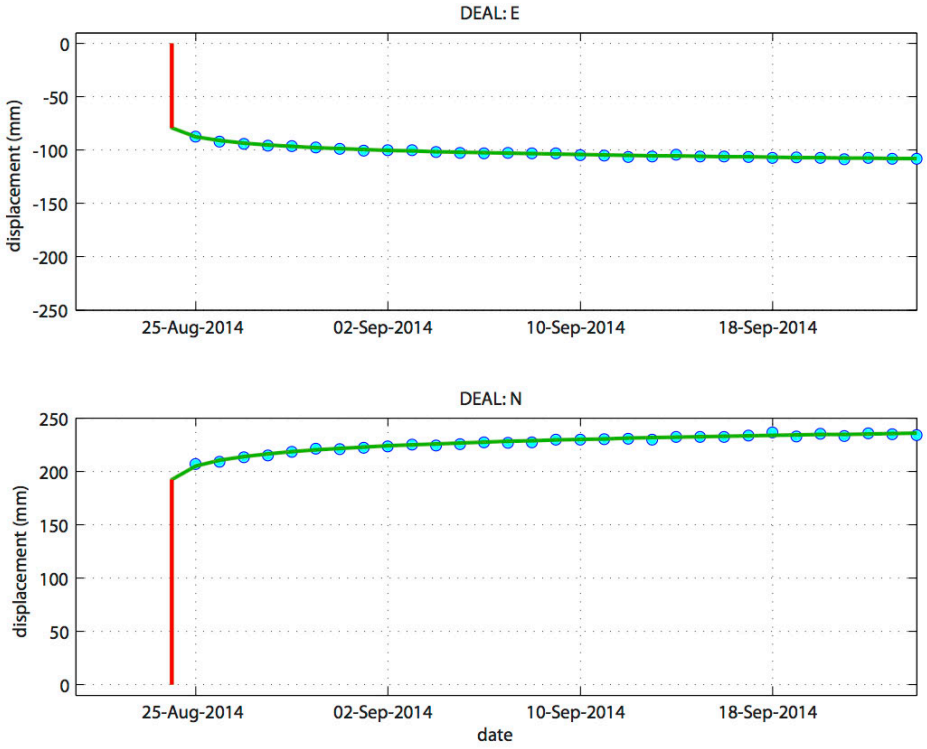

Figure 10. Graph showing postseismic displacement for GPS station DEAL, closest to the West Napa Fault near Napa, Calif.

Under the assumption that all postseismic deformation observed with GPS during the first two months following the earthquake is due to fault slip, we have used the GPS and alinement array data to jointly estimate the slip that occurred on August 24, 2014, and the cumulative slip over the first two months following the earthquake. In this preliminary model, most postseismic observations can be fit with afterslip concentrated in the upper 3 km. Given the magnitude of displacements recorded to date from the GPS stations and alinement arrays, and the steadily decaying postseismic velocities at these measurement sites, it seems unlikely that cumulative postseismic offsets at the fault trace will ultimately reach the >1 meter of coseismic slip inferred from GPS to have occurred at depths greater than 1 kilometer on August 24, 2014.

The GPS station spacing in the region is large relative to the length of the fault rupture, limiting the degree to which details of the coseismic slip distribution and any afterslip can be resolved. SAR interferograms spanning the postseismic period provide better spatial coverage and may record other processes, such as poroelastic effects, whose signals are also present in the GPS data. Therefore the clear postseismic signals may not be entirely attributable to afterslip, which could in turn reduce the expected amount of ongoing displacement that fault crossing structures will experience. Further analysis of the time dependent displacement may shed light on fault zone characteristics, such as frictional properties, that influence the magnitude and spatial extent of afterslip. Ongoing modeling is focused on these questions.

In the next section of the report, we further examine the issue of how best to fit the GPS and alinement array data in order to forecast the long-term afterslip. First, this is done for all of the data, and then with particular attention to the observations from closest to Browns Valley.

Summary

South Napa earthquake data from four alignment arrays, seven campaign GPS sites, and one continuously recording GPS site have been analyzed using various methodologies presented in the literature characterizing the observed postseismic slip following earthquakes. Given that only 80 days had elapsed since the mainshock on August 24, 2014, at the time of this analysis, the short interval of data precludes unambiguously determining an appropriate function for extrapolating postseismic deformation into the future. Figure 11 (*A*, *B*) shows the range in functions that fit most of the observations made within 3 months after the earthquake and the predictions by these functions of displacement over the next 30 years. Consequently, depending upon the function (fig. 11*A*), one might expect that the postseismic deformation could increase by 15 to 100 percent. On the other hand, examination of data collected after other earthquakes that have produced postseismic slip, most notably the 2004 *M*6 Parkfield earthquake, suggests that although each of these functions tends to characterize the observations made within a half year of the mainshock, only those functions that have rapidly decreasing rates of deformation after one year tend to fit the observations over the long term.

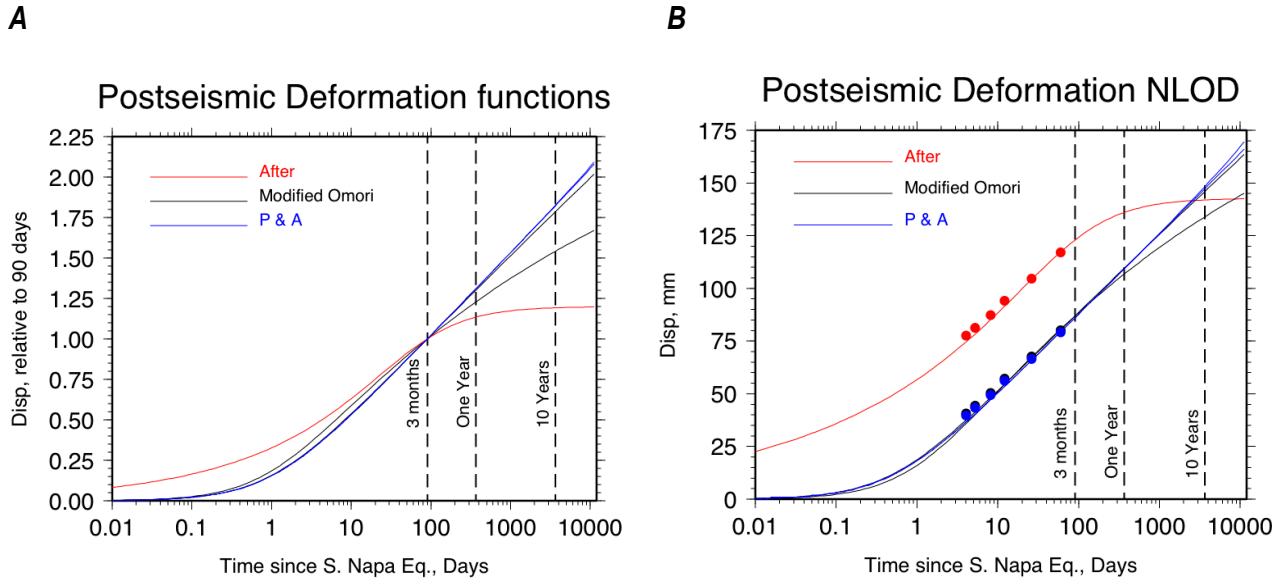

Figure 11. Plots showing postseismic deformation following the August 24, 2014, South Napa earthquake. *A*, Plot of three different functions used to fit a combination of alinement array and GPS data collected in the 3 months following the South Napa earthquake. These functions have been normalized such that they all intersect at 90 days. For periods beyond 3 months, the curves are extrapolations. Two curves are shown, one with power law index of 1, called Omori law, and a second curve with an index of 1.1, called the modified Omori law. [AFTER and P & A are defined on the next page.] *B*, Same functions as *A* but rescaled to fit the data from alinement array site NLOD located at Leaning Oak Drive. Data from NLOD are plotted, but because the observations start 5 days after the mainshock, the absolute datum is shifted dependent upon the functional model of deformation. For instance, the AFTER (fig. 11*A*) model suggests that at 5 days, approximately 60 percent of the 90 days of deformation has occurred, but for the modified Omori, 45 percent of the slip occurred.

As an example, alinement array site NLOD has seen 40 mm of slip between 5 and 60 days following the South Napa earthquake. Rescaling those observations (fig. 11*B*) and extrapolating the curves to 30 years suggests between 140 and 170 mm of postseismic deformation will have accumulated

since the time of the earthquake. However, this type of estimate assumes that we can correctly shift the datum of these observations such that the amount of slip between the time of the mainshock and the first observation is correctly estimated.

Models

Three different functional relationships have been used to characterize the time dependence of the observed postseismic deformation. These include AFTER (Boatwright and others, 1989; Budding and others, 1989; Lienkaemper and others, 2006), the modified Omori law (for example, Langbein and others, 2006), and a function derived by Perfettini and Avouac (2004) called P & A, which is included in Langbein and others, 2006. The AFTER function has been used successfully for over 25 years to describe alinement array observations of postseismic slip. It has two terms that characterize the power-law time dependence, tau and the temporal index, p. Its chief characteristic is that once time (t) > tau, the deformation nearly ceases, which is in contrast to both the modified Omori law and the P & A functions. The modified Omori law is derived from the observed power-law rate-dependence of earthquake aftershocks. In addition, it is related to power-law creep of a spring and block slider model (Montesi, 2004). Likewise, the P & A function is a derivation based upon a spring and block model of creep characterized by a rate-state friction law. Like the AFTER function, both of these functions have two parameters that describe the time-dependence, but the time constant for these two functions physically describes the delay in the onset of postseismic deformation following the mainshock and not the length of the postseismic interval. With high sample-rate data, which is only provided by networks with telemetry, it becomes possible to infer time of the onset of postseismic deformation (Langbein and others, 2006). Consequently, for both the modified Omori and P & A functions, only one parameter describes the long-term deformation.

Data

Three different sets of observations characterize the postseismic deformation (fig. 8). Alinement array measurements of slip from the South Napa earthquake at four sites (fig.14) commenced between 1 and 5 days after the mainshock and include approximately one-half dozen observations over the following 2 months (with another set of observations just completed in late November 2014, which are not included in the present analysis). Previous analysis by J. Lienkaemper (written commun., 2008) suggests that typical data from alinement arrays located throughout northern California have a short-term repeatability of better than 1 mm/√yr and 2 mm/√yr of random walk owing to a combination of monument stability and variations in creep rate. The most recent analysis of the precision of the Napa alinement array data is consistent with the previous analysis (J. Lienkaemper, written commun., 2008), with short-term repeatability ranging between 0.3 and 1.3 mm; in addition, 2 mm/√yr of random walk is added to the error budget but has only minor impact owing to the shortness of the time series.

Campaign style GPS was initiated about 1 day after the mainshock and includes observations through early November 2014. To improve their temporal resolution, the receivers have been "semipermanently" installed at a number of these sites. Except for one site, DEAL, these sites are located more than 5 km from the fault trace that has been actively slipping. Seven sites that are closest to the active creep and exhibiting a clear signal related to postseismic deformation are analyzed here. Although detailed analysis of the observational error of these data has not been done, 1 mm of white noise and 2 mm/√yr random walk are provisionally used.

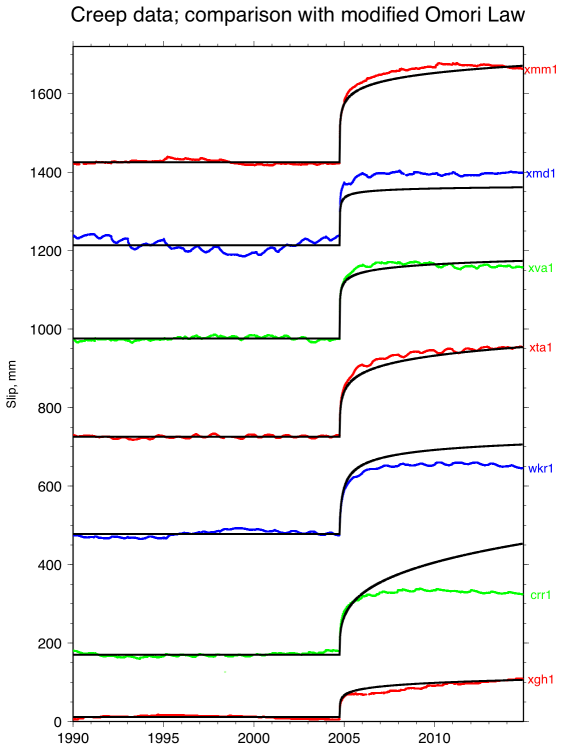

Figure 12. Graph showing creepmeter data compared with the modified Omori law. Creepmeter data spans the 2004 Parkfield earthquake and shows 10 years of postseismic slip. Secular rates are removed from creep data (between 3 and 12 mm/yr). The black curve is the best fit, modified Omori law based on a combination of 10-minute and daily observations of creep for an interval through 2005.5. The black curves after 2005.5 are extrapolations.

The Plate Boundary Observatory, operated by UNAVCO, has many continuously recording GPS sites throughout northern California. Unfortunately, their coverage is sparse in the area around Napa. (Only one site, P261, has modest, ~1 cm, postseismic deformation.) Scientists at the USGS in Menlo Park processed those data, both to produce estimates of position once per day and also at 5-minute intervals. The short-term precision of the 5-minute samples ranges between 2 and 5 mm, in contrast to the 0.8-mm precision of the 24-hour (daily) observations. In addition, both data types have a temporal error that has been factored into the analysis.

Method

For each of the functions, a coarse grid search was employed to estimate the two temporal parameters of the selected function. Then, for each combination of temporal parameters, the function was fit to each time series of observations by using least squares to estimate the optimal amplitude (and other terms that are relevant to characterize the deformation spanning the interval prior to, during, and after the earthquake). The misfit of the data in the least-squares adjustment was normalized relative to the data error (or covariance) and tabulated as chi^2. The value of chi^2 was summed both over each choice of the temporal coefficients and for each functional type. Table 2 summarizes the fit to each data type.

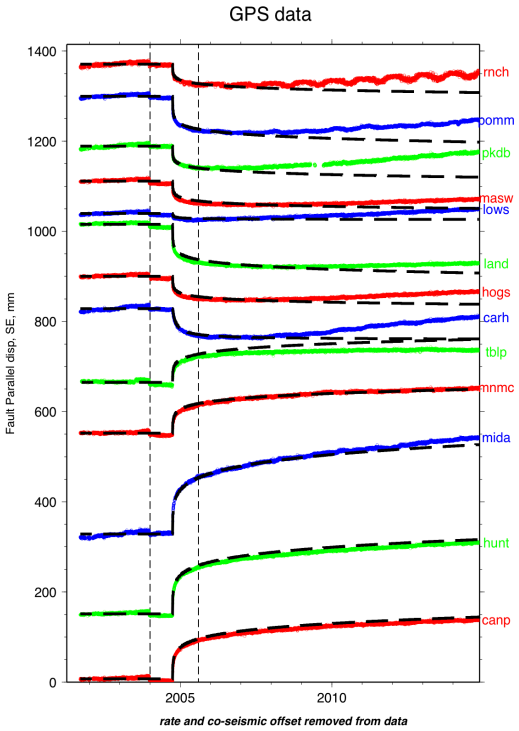

Figure 13. Graph showing fault parallel displacements derived from continuously recording GPS data relative to site CRBT, located ~50 km west of the San Andreas Fault. These data, which only became available in mid-2001, span the Parkfield earthquake (2004.7) and the San Simeon earthquake (2003.9). The dashed black curve is the best fitting modified Omori law using a combination of high-rate, 10-second samples and daily samples of positions. The curve was derived based on observations made prior to 2005.5, thus, the curves after 2005.5 are extrapolations. The orientation of the data is reversed because half of the sites are located on the west side and half the sites are located on the east side of the fault.

Other Constraints

Both creepmeter and continuously recording GPS data spanning the 2004 Parkfield earthquake provide some guidance as to which of the three models are most appropriate for characterizing postseismic deformation in the decade following the mainshock. Langbein and others (2006) successively fit both modified Omori and P & A functions to both creepmeter and continuously recording GPS. Because these data are telemetered, high-rate sampling of fault slip and position changes is possible. Creep has been sampled at 10-minute intervals since the mid-1980s. In mid-2001, continuously recording GPS was installed at 14 sites in the Parkfield area. By mid-2003, the sampling interval was decreased from 15 to 1 second, and positions were estimated in real time at 1-second intervals. High-rate sampling of creep and GPS position made it possible to precisely delineate coseismic and postseismic intervals; Langbein and others (2006; fig. 13) clearly showed that postseismic slip was delayed by approximately 1 hour after the mainshock. Because this observation is not predicted by the AFTER function, that function was rejected in favor of either the P & A or modified Omori function. Langbein and others (2006) used the available creep and GPS data through

mid-2005 to fit P & A and modified Omori functions to the data. However, examination of figures 12 and 13, which show the creep and GPS data through late 2014, indicates that the modified Omori law tends to overestimate the amount of postseismic deformation (the same occurs for P & A, too).

Remarks

Figure 11 (*A*, *B)* suggests a wide range in possible postseismic deformation extrapolated out to 30 years. This reflects the epistemic uncertainty in defining the appropriate function to represent postseismic deformation. Tabulation of the chi^2 statistics for fitting the observations to each of these models indicates a slight preference for the AFTER function. The epistemic uncertainty is greater than the formal statistical uncertainty in any of these functions. Perhaps a better discriminant is provided by examining a decade of Parkfield postseismic observations. These tend to favor the AFTER function over the long term, even though AFTER can be rejected for characterizing the postseismic deformation for the first day following the mainshock.

We cannot be certain that the San Andreas Fault at Parkfield, for which we do have data, has behavior similar to the West Napa Fault System, for which we have only three months of data so far (since occurrence of the South Napa earthquake). The San Andreas provides, however, the best analogy available that has data allowing us to model expectations for afterslip following the South Napa earthquake.

Table 2. Chi-squared statistics of misfit for functions describing postseismic deformation.

Data type	Number of observations	Chi^2 of misfit relative to data covariance		
		AFTER	Modified Omori	P & A
Alinement array	22	15.91	<u>13.95</u>	15.22
Campaign GPS	376	<u>482.74</u>	486.61	484.82
Continuous GPS; mix of 5-minute and daily data.	3,651	<u>3989.28</u>	3991.51	3991.84

Best fit is <u>underlined.</u>

Alinement Array Data and Afterslip Forecasts

Alinement arrays were established along the main fault trace, as well as on one of the eastern fault strands (Lienkaemper and others, 2014) soon after the earthquake (fig. 14). The data from these alinement array surveys may be used alone instead of in combination with GPS and other data, as was done in the previous section of this report. In the next part of this report, the alinement array data are described in greater detail. The AFTER program (Boatwright and others, 1989; Budding and others, 1989; Lienkaemper and others, 2006) is then used to systematically produce forecasts for the afterslip, that is, extrapolations based on the data to a point in the future. Because of the uncertainty about the best type of function to use in forecasting the afterslip, we examine the alinement array data on its own and produce forecasts using only the formal errors put out by the AFTER program. These formal uncertainties are much smaller than the total range of uncertainty values explained in the previous section, which attempted to take into account the unexpected unknowns. In the next section, we address the expected unknowns and make forecasts using the AFTER function form that flattens much faster with time than the other functions described earlier.

"The main rupture was ~15 km long from its epicenter (defined here as km 0, see [fig. 14]) to the surface rupture's north end (~km 15). Near km 10, a maximum of ~0.45 m right-lateral fault slip was most likely entirely coseismic, because it showed the same amount of slip at 12 days post-earthquake (d-PE) as it did at 1.5 d-PE. However, farther south (km~6) by 1-2 d-PE, conspicuous growth of offsets on cultural features indicated high rates of afterslip (~10-20 cm/day) had occurred. Although afterslip is gradually slowing, it is expected to continue for many months or possibly years. To closely monitor this rapid afterslip, [Lienkaemper and others (2014)] installed four 70-140-m-long alinement arrays across the main rupture (labeled NLAR-NLOD on [fig. 14]), measuring slip to millimeter accuracy. A fifth array that spans a northeastern branch rupture has shown no afterslip. [Lienkaemper and others (2014)] have run early observations (to 26-d-PE) of afterslip (coupled with accumulated total slip as measured on adjacent offset cultural features) in the program AFTER (Boatwright and others, 1989). This analysis allows [Lienkaemper and others (2014)] to make preliminary estimates of initial (1 d-PE), final or total accumulated event slip, and coseismic estimates (that is, projecting slip toward a ~0.5-1 s rise time). Thus far modeled slip on all four arrays indicates that final values of total (coseismic plus post-seismic) slip might be approaching the maximum coseismic slip as a limit (~0.4 ± 0.1 m). The final values of total surface slip may thus become more uniform along the fault over time as compared to modeled heterogeneous seismic slip at depth. The timing of the surface slip release differs strikingly from south to north along the 2014 rupture; AFTER models suggest that slip south of the location of maximum slip (km 0-10) appears to have been dominantly postseismic (~50-100%), whereas north of the maximum slip (km 10-15) slip was mainly coseismic (~50-100%). The current AFTER model predicts that as surface slip along the fault approaches final values of total slip associated with this earthquake (*for example,* ≥1000 d-PE), the respective contributions to the total event surface slip integrated along the entire fault will approach being 27% coseismic slip and 73% postseismic slip."

The above quote is directly from Lienkaemper and others (2014). The following three figures, citing the same Lienkaemper and others (2014) AGU abstract source, are updated as of November 25, 2014, and their inclusion in this report was allowed by written communication with James Lienkaemper (USGS), 2014. In addition, data from the most recent field survey, performed on November 21, 2014, are included in figures 15 and 16 along with a summary of the most recent calculations. To summarize the results of Lienkaemper and others (2014), if one considers only the alinement array data and AFTER model forecasts and their formal uncertainties, most of the afterslip has already occurred now that three months has elapsed since the South Napa earthquake.

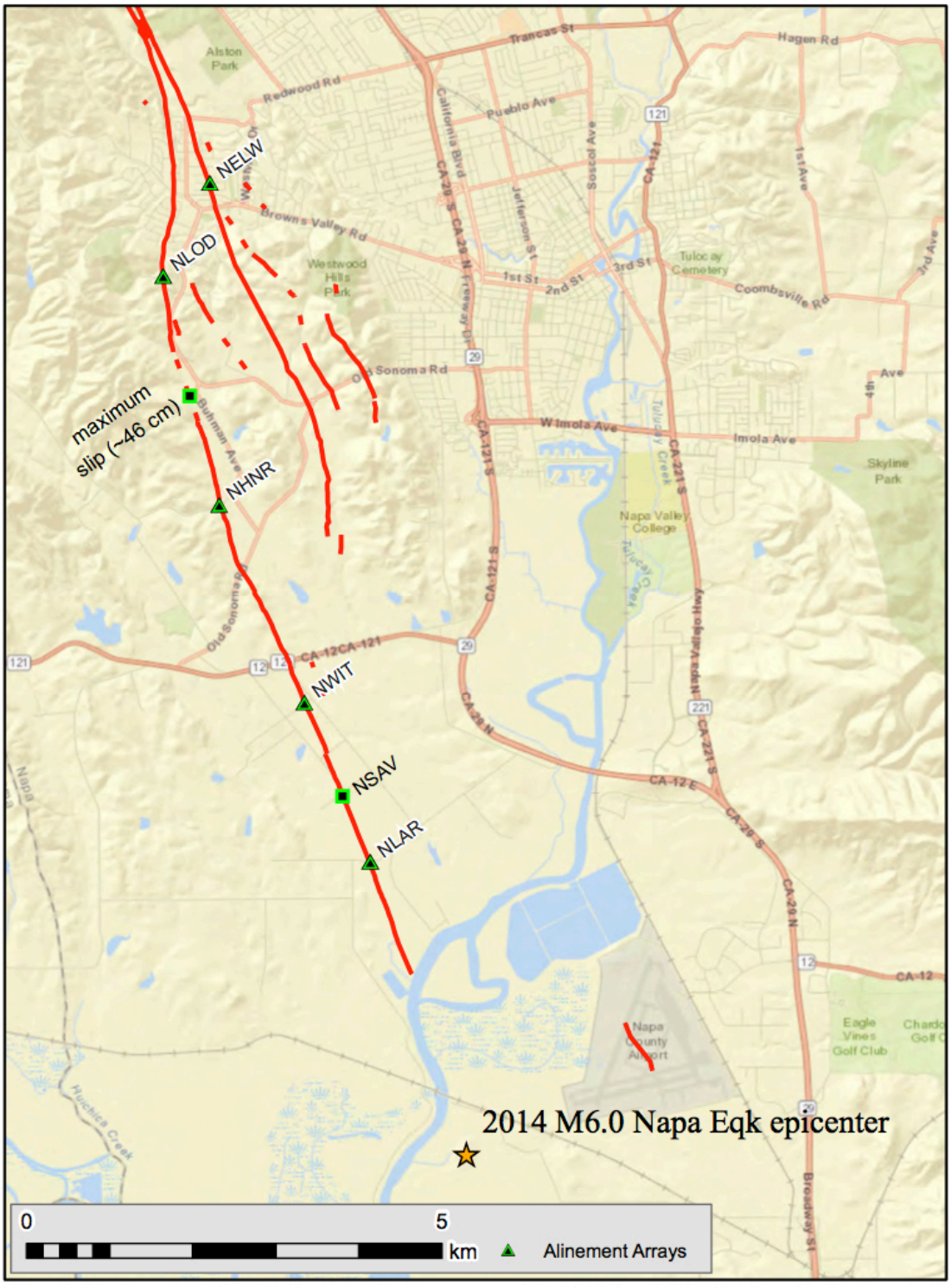

Map of alinement arrays installed across surface ruptures of the M6.0 South Napa Earthquake that occurred at 3:20 AM PDT on Aug. 24, 2014.

Figure 14. Map showing USGS alinement arrays installed across surface ruptures of the *M*6.0 South Napa earthquake, from Lienkaemper and others (2014).

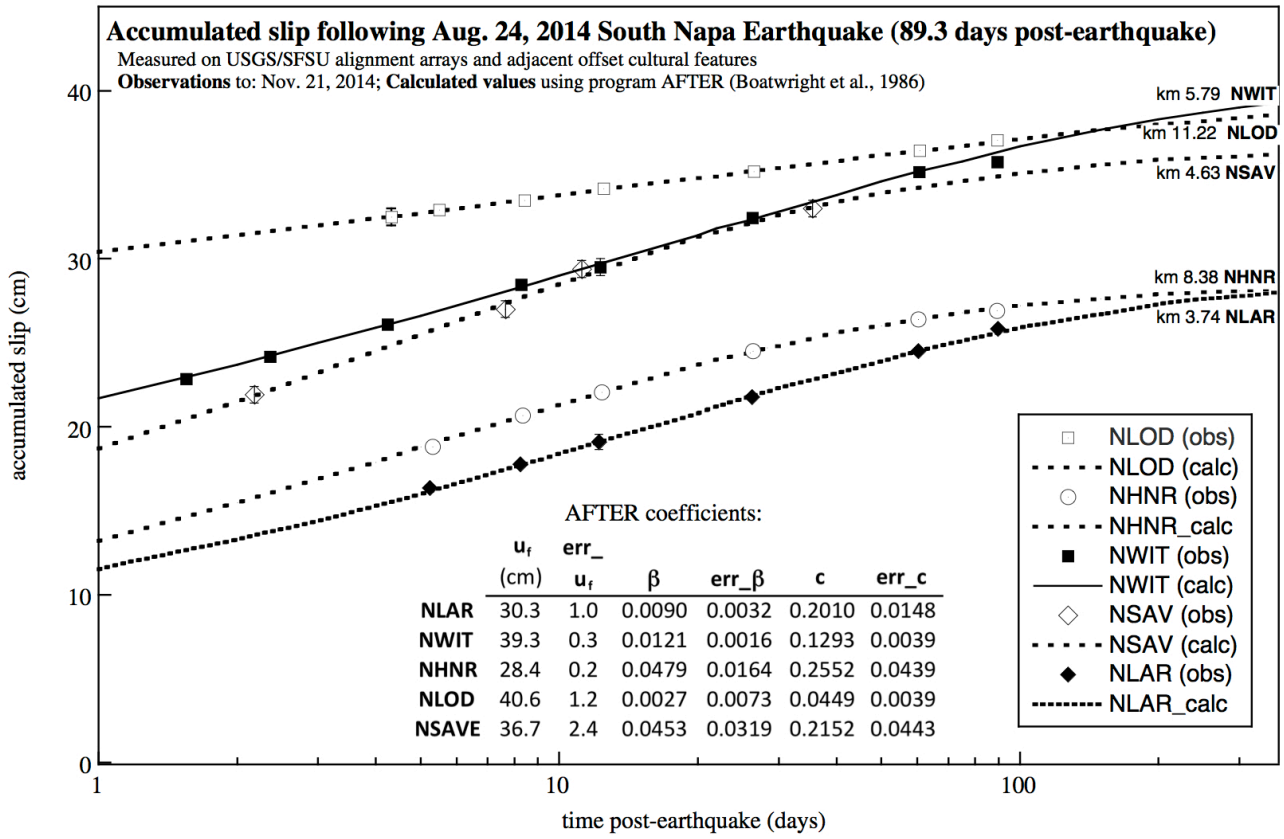

	u_f (cm)	err_u_f	β	err_β	c	err_c
NLAR	30.3	1.0	0.0090	0.0032	0.2010	0.0148
NWIT	39.3	0.3	0.0121	0.0016	0.1293	0.0039
NHNR	28.4	0.2	0.0479	0.0164	0.2552	0.0439
NLOD	40.6	1.2	0.0027	0.0073	0.0449	0.0039
NSAVE	36.7	2.4	0.0453	0.0319	0.2152	0.0443

Figure 15. Afterslip forecasts showing data, curve fits using the AFTER program, and a tabulation of fit parameters and formal uncertainties forecast for each alinement array, from Lienkaemper and others (2014).

Afterslip Within the Browns Valley Neighborhood

Only one example of the many interferograms that were examined is provided in this report in the interest of brevity. A vast amount of geospatial information was used to determine which portions of the West Napa Fault Zone broke in the earthquake and which sections continued to experience afterslip in the weeks and months since the earthquake. For the forecasts of future afterslip in the residential areas, we rely most heavily on the GPS and alinement array data. The following sections of this report describe the use of these data to examine afterslip along the entire fault rupture, and then on the portion of the fault in Browns Valley.

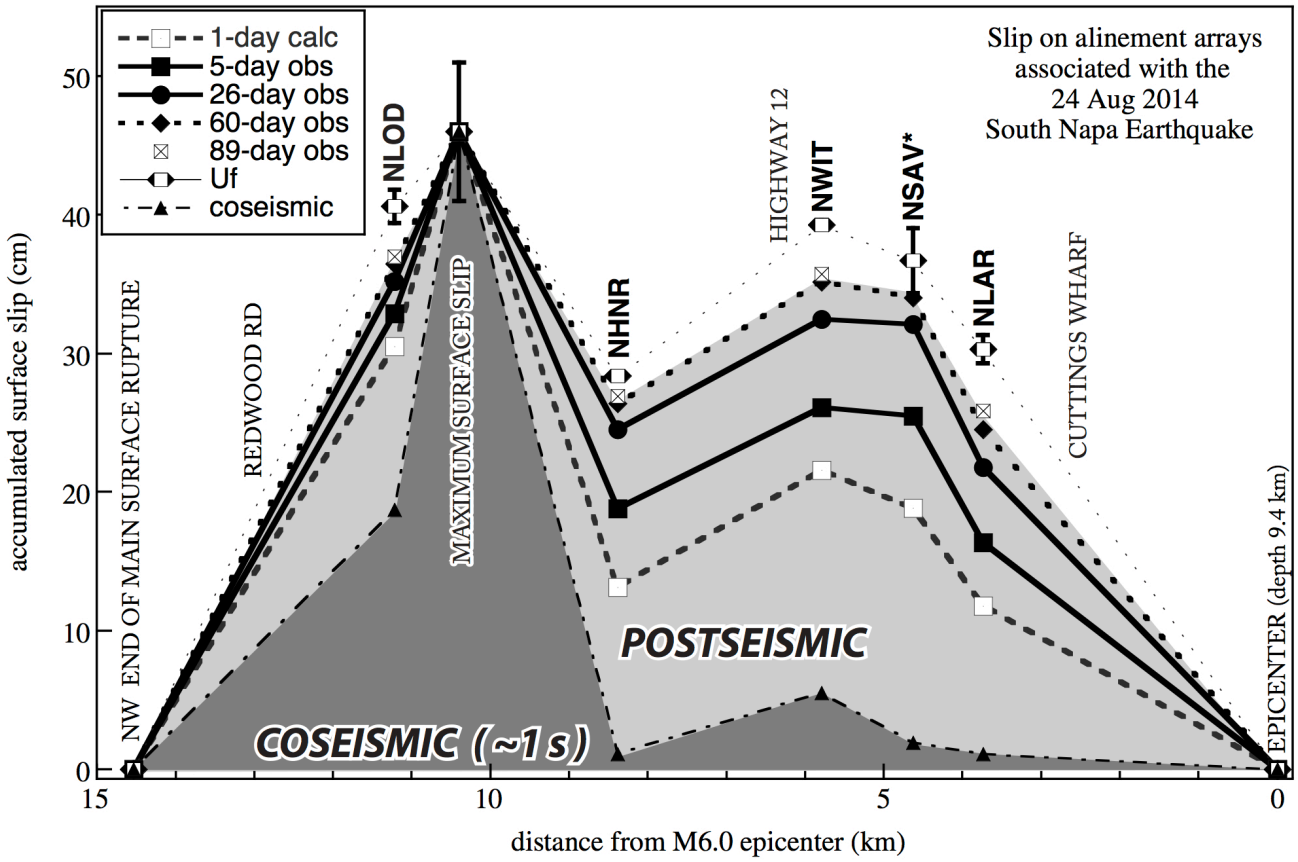

Figure 16. Summary graph of alinement array data. The epicenter is at the right, and the Browns Valley neighborhood is near the left side from the NLOD array at 11.5 km on the x-axis, running to the left (north) up to a point south of Redwood Road at 13 km on the x-axis. Coseismic slip is shown by the lower, dark-gray curve. Afterslip is shown by the upper family of curves that increase with time after the mainshock. The alinement array NLOD is at Leaning Oak Drive at the south end of the Browns Valley neighborhood. From Lienkaemper and others (2014).

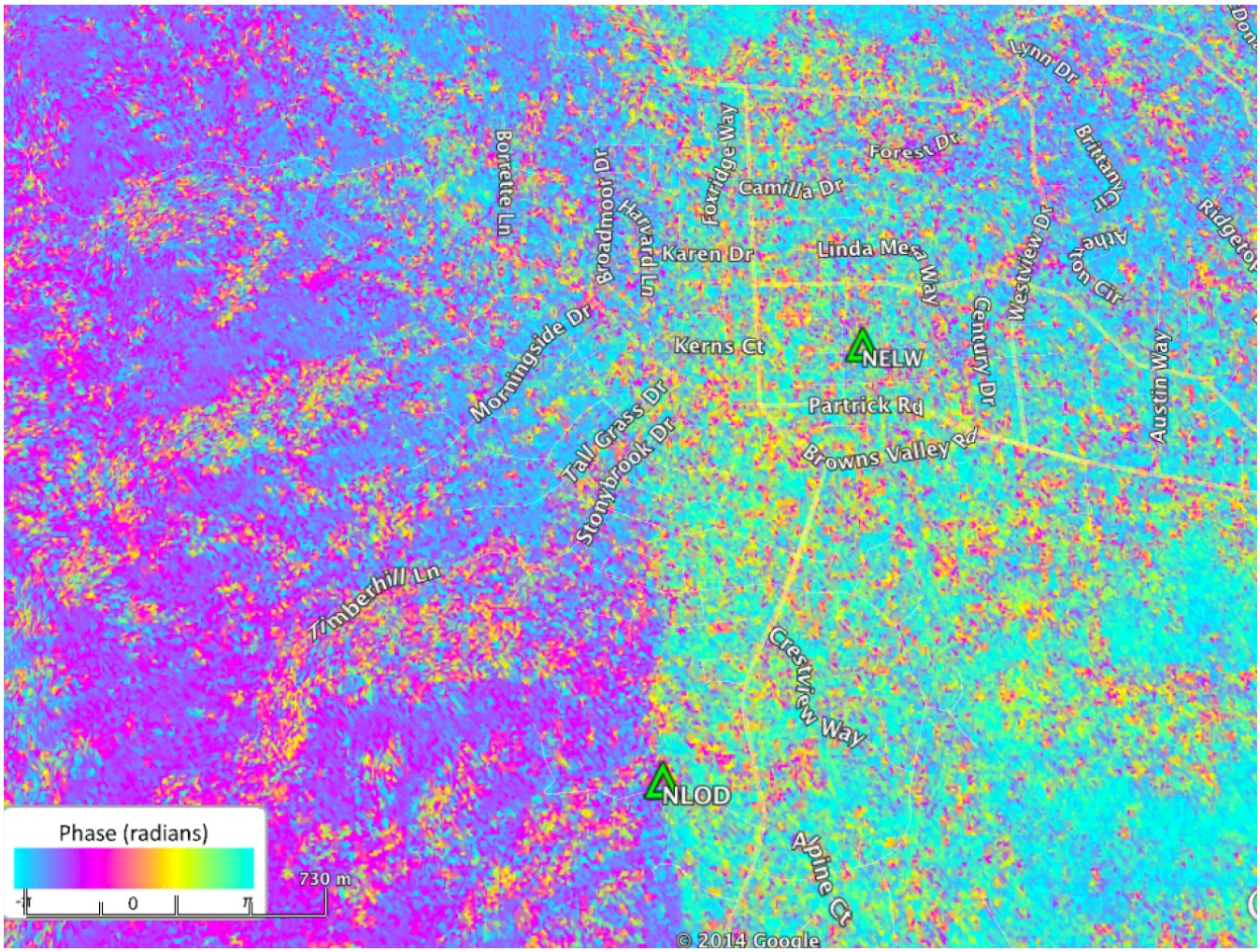

Figure 17. Uninhabited Aerial Vehicle Synthetic Aperture Radar (UAVSAR) image of afterslip along a part of the main West Napa Fault strand in the Browns Valley neighborhood. From Leaning Oak Drive (NLOD) USGS alinement array site toward the north, afterslip is clearly visible as a break between purple and blue pixels west of the main fault strand and light green pixels east of the main fault strand. No afterslip is observed in this image (or any other images we have analyzed) along the eastern strand that is marked by NELW, the USGS alinement array. UAVSAR postseismic deformation image provided by JPL; single interferogram, August 29, 2014, through October 22, 2014. UAVSAR Track Number 05512. Color scale is 23.79 cm (full wavelength). Source of image is National Aeronautics and Space Administration, Jet Propulsion Laboratory, California Institute of Technology. Standard browse image accessed from *http://uavsar.jpl.nasa.gov/*. [See also Donnellan and others (2014) and *http://www.jpl.nasa.gov/news/news.php?release=2014-306*.]

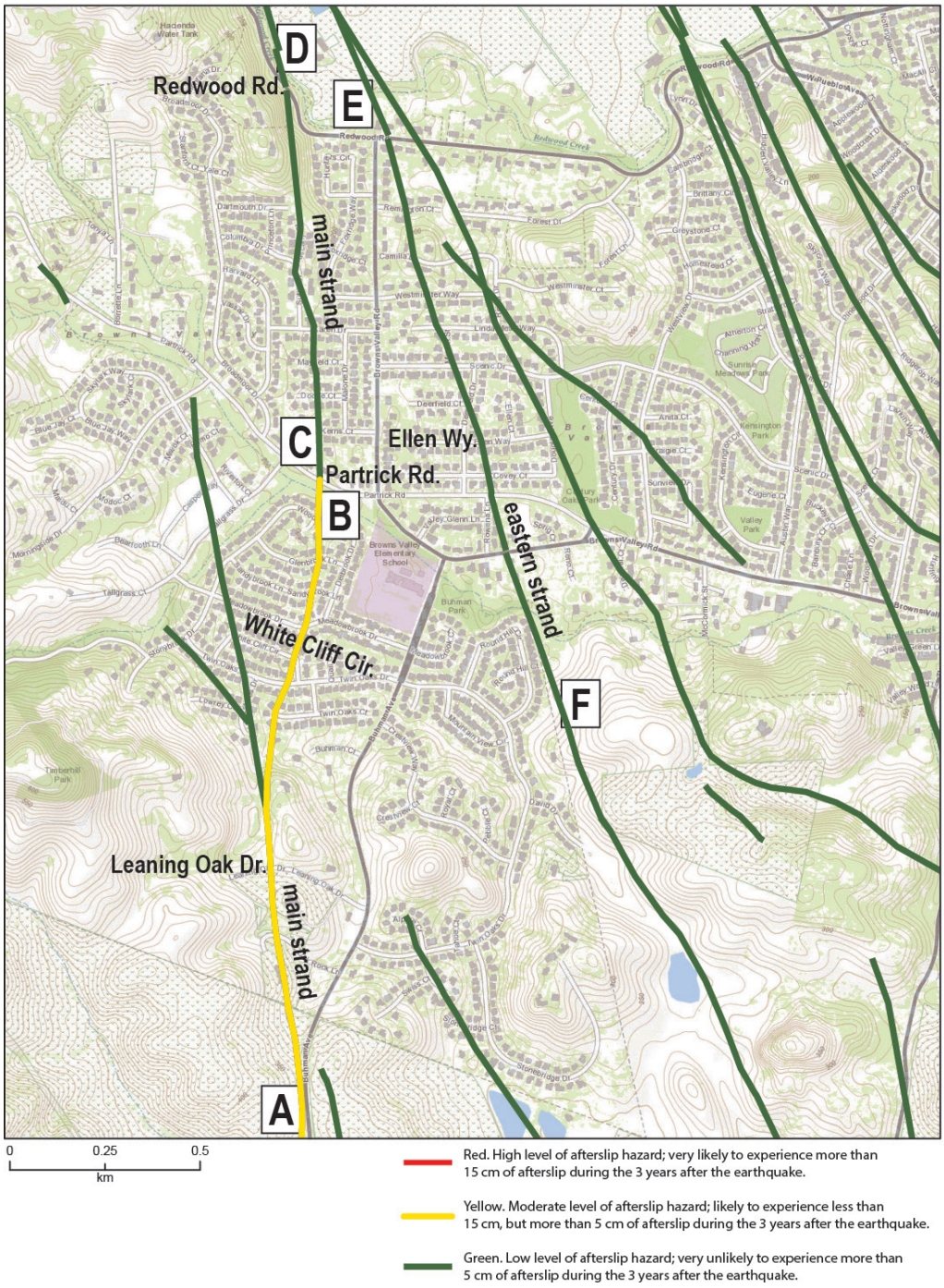

Figure 18. Map of Browns Valley neighborhood with fault traces and other lineaments showing levels of afterslip hazard. All of the faults and/or imagery lineaments shown as heavy green lines on this map may be considered to have a low level of afterslip hazard. The UAVSAR image in figure 17 shows that afterslip extends northward, but with a steadily decreasing amount, up to the intersection of the main fault strand with Partrick Road, located at lat 38.307273° N., long 122.342632° W. From that point to the north, there is no evidence for afterslip, so that section of the fault is rated low afterslip hazard. Similarly, the eastern strand of the fault is rated low afterslip hazard on the basis of data from the NELW array, and imagery shows that no afterslip has occurred within 3 months since the mainshock. All fault strands shown, however, are potentially susceptible to fault slip in future earthquakes.

A copy of figure 18 accompanies the Executive Summary. All fault traces shown on this map face potential future earthquake fault surface rupture hazard and other earthquake-related hazards such as shaking, liquefaction, and landslides; these hazards are treated separately in other publications and maps from CGS and USGS. For all levels of afterslip hazard, the afterslip amount that is measured 90 days after the earthquake can be expected to as much as double by 10 years after the earthquake (less than double is also possible). The southern part of the main strand of the West Napa Fault within Browns Valley, from south of Leaning Oak Drive up to Partrick Road (A to B on map), that is shown in yellow on the accompanying map, is forecast to experience continued afterslip of an amount that is estimated in detail in previous sections this report. Although the forecasted afterslip in the southern part of the Browns Valley neighborhood (A to B in yellow on map) from Leaning Oak Drive to Partrick Road poses an ongoing hazard to structures, the amount of afterslip is not so great as to pose a highly severe ongoing hazard. The afterslip and associated hazard decreases exponentially with time, posing a moderate hazard.

The northern part of the main strand of the West Napa Fault within Browns Valley, north of Partrick Road (C to D on map), has experienced no significant afterslip; low afterslip hazard exists on this part of the main strand of the West Napa Fault System. The newly named "eastern strand" of the West Napa Fault System (E to F on map) has experienced no afterslip along the sections shown in figure 18; low afterslip hazard exists on this part of the eastern strand.

Other fault strands shown in green on figure 18 also have low afterslip hazard. Subsequent ongoing mapping, that is, work still in progress, may reveal that certain lineaments shown here are not actually faults.

Categories for severity of fault afterslip:

Red Fault Trace—High level of afterslip hazard; very likely to experience more than 15 cm of afterslip during the 3 years after the earthquake.[10]

Yellow Fault Trace—Moderate level of afterslip hazard; likely to experience less than 15 cm, but more than 5 cm, of afterslip during the 3 years after the earthquake. [11]

Green Fault Trace—Low level of afterslip hazard; very unlikely to experience more than 5 cm of afterslip during the 3 years after the earthquake.[12]

For all levels of afterslip hazard, the afterslip amount that is measured 90 days after the earthquake can be expected to as much as double by 10 years after the earthquake.

[10] In this case, no red is indicated.

[11] In this case, additional afterslip accumulation is likely to gradually accumulate an additional 5 cm during the 10 years after the earthquake and an additional 5 cm 30 years after the earthquake.

[12] In this case, faults that experienced <10 cm of coseismic offset and <5 cm of afterslip within the 3 months after the earthquake are included in this category. Some faults or lineaments shown as green had no measurable coseismic slip or afterslip associated with the August 24, 2014, earthquake. Faults and lineaments of several categories are shown for completeness. Some are previously mapped strands (U.S. Geological Survey and California Geological Survey, 2006); others represent preliminary mapping based on a combination of imagery interpretation and field mapping that has taken place since the August 24, 2014, earthquake.

Fault Hazards

The M_w 6.0 South Napa earthquake of August 24, 2014, was associated with surface rupture along fault traces of the West Napa Fault System (WNFS; fig. 19). This fault system is part of the broader San Andreas Fault System that extends across the San Francisco Bay region and northern California. In the UCERF 3 (Field and others, 2014) characterization of California faults for the National Seismic Hazard Map, the West Napa Fault was modeled as producing a $M \geq 6.7$ earthquake every 1,153 years and as having an estimated slip rate of 2 mm/yr. However, there are few actual constraints on the earthquake behavior of the WNFS. There are no independent geologic estimates of the recurrence time of large earthquakes, the maximum size earthquake, the amount of surface slip that the fault system can produce, or the fault slip rate across and along the Napa Valley.

Faults included in the WNFS had been recognized and mapped as having slipped in the Quaternary (USGS and CGS, 2006), but most of the fault system has not been studied well enough to document Holocene displacement sufficient to recognize the WNFS as a significant surface-faulting hazard. The State of California requires that a fault be sufficiently active and well-defined as to constitute a potential hazard to structures from surface faulting or fault creep to be zoned under the Alquist-Priolo Earthquake Fault Zoning Act (California Public Resources Code 2622). For the WNFS, only a short 8-km segment extending south from the Napa County Airport had received this designation prior to the South Napa earthquake of 2014. Nearly all of the 2014 surface rupture occurred north and west of the Napa County Airport on faults that had not previously been recognized as active during the Holocene (fig. 21). Parts of the 2014 surface rupture were also located in areas where no faults had previously been mapped.

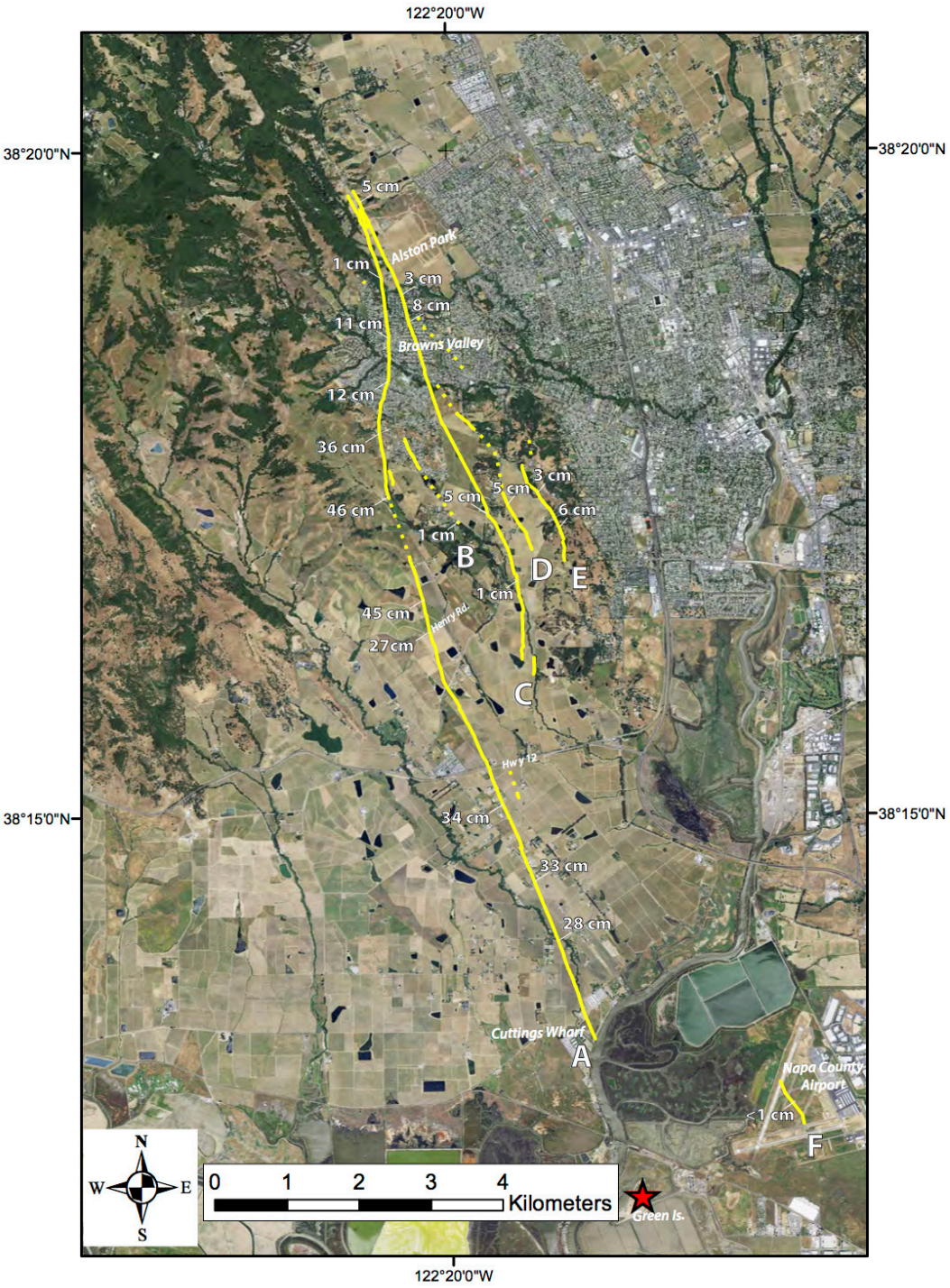

Figure 19. Map showing traces of tectonic surface faulting (yellow lines) produced by the August 24, 2014, South Napa earthquake. Right-lateral surface displacements, measurable in the field, were observed along traces labeled A–F. Solid lines indicate regions where surface faulting was observed to be relatively continuous. Dotted lines indicate regions where surface faulting was discontinuous, diffuse, or where lateral displacements were negligible. Numbers show maximum measured right-lateral offset at selected sites, rounded to the nearest cm; includes both coseismic as well as measured afterslip as of November 17, 2014. Red star is location of earthquake epicenter.

Surface faulting extended at least 12.5 km from the Napa River at Cuttings Wharf northward beyond the northern boundary of Alston Park in the City of Napa (fig. 19). Faulting occurred on two principal subparallel north- to northwest-trending fault strands (traces A and C, fig. 19). Geologists identified four additional minor, subparallel fault ruptures (less than 1.5 km in length); these are noted as traces B, D, E, and F (fig. 19). Surface rupture lies almost entirely northwest of the epicenter (red star on figure 19) and, fortunately, was largely confined to agricultural areas with relatively sparse infrastructure. The exception was in the Browns Valley area, where relatively small surface displacements produced considerable damage.

In addition to confirmed tectonic surface rupture, areas of ground cracking with little measurable displacement were also observed, some along linear trends as far south as Green Island and to the north for more than 1 km beyond where tectonic surface faulting has been confirmed. One of these zones occurs in Browns Valley to the east of trace C and is shown on figure 19. Some of these anomalous ground cracks may be related to tectonic faulting, but most can be explained by shaking-produced ground lurching, lateral spreading, differential settlement, or bedding-plane-controlled ridge-top spreading.

Surface displacements are predominantly right-lateral and typically expressed as discontinuous, en echelon, left-stepping fractures within zones from <1 m to as much as tens of meters in width (fig. 20). The largest lateral offsets occurred on trace A (fig. 19); fault slip was minimal near the epicenter, reaching a maximum observed displacement of 46 cm approximately 10 km to the northwest. Slip decreased progressively to the north from there, but in the Browns Valley area, offsets of 10–20 cm across roads, pipelines, and residential structures produced significant damage. Trace C also crosses through Browns Valley, where right-lateral offsets of 2–8 cm were observed. Near the northern end of the rupture zone, traces A and C approach each other and may merge north of Alston Park. Right-lateral offset of approximately 6 cm was also measured on trace E. The amount of offset on the other two surface traces is 5 cm or less and could not be precisely measured in the field in most locations.

As discussed previously, the total amount of slip documented to date on trace A evidently occurred both coseismically and as afterslip. Most of the total displacement was produced by afterslip south of Henry Road (NHNR on figure 14 and annotated at center of figure 19), whereas, to the north, most of the slip appeared to have occurred coseismically. Afterslip was most rapid in the middle third of trace A, increasing initial slip by ≥20 cm 1 day after the mainshock. Repeated measurements suggest total slip may reach ~40 cm along half of trace A. Afterslip was looked for but not observed on trace C (alinement array NELW). Whether afterslip occurred on the shorter ruptures is unclear, although delayed reports of cracking across Old Sonoma Road and an associated water main break that was not reported immediately after the earthquake opens the possibility of a small amount of afterslip having occurred on trace E.

Figure 20. Photographs showing ground surface features resulting from fault displacement during the South Napa earthquake. *A*, Left-stepping en echelon fractures on trace A characteristic of right-lateral fault displacement at the ground surface. Right-lateral displacement of 40 cm was measured near this location one day following the earthquake. Photograph by Dan Ponti, USGS. *B*, Small displacement ground cracks along trace A near Cuttings Wharf Road, south of Highway 12, taken the day of the earthquake. Displacement in this area grew to ~20 cm in a right-lateral direction by Monday, August 25, 2014, owing to afterslip. Photograph by Ben Brooks, USGS. *C*, Right-lateral offset of Browns Valley Road centerline, on trace C. Photograph by David Schwartz, USGS.

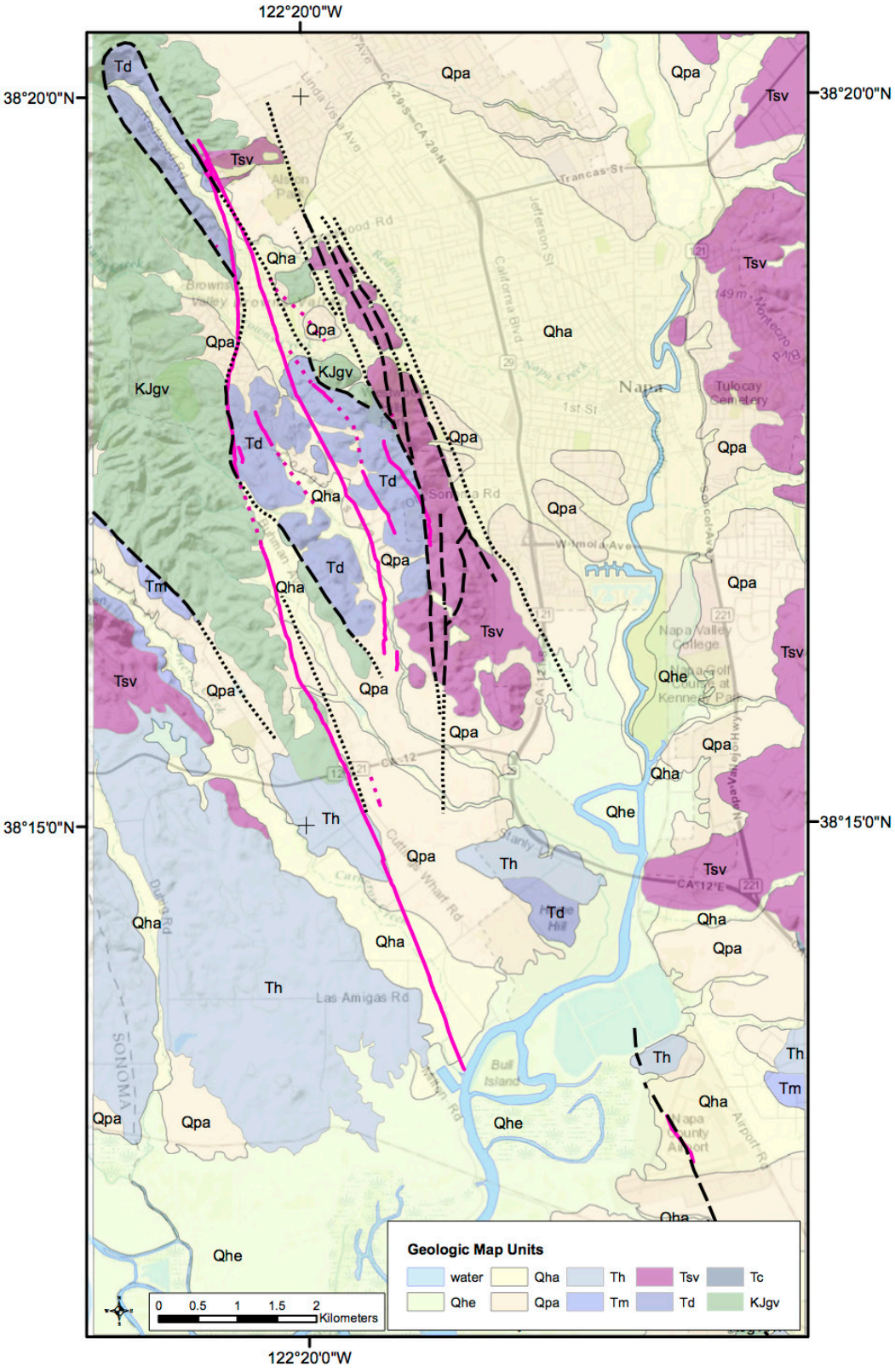

Caption follows on next page.

Figure 21. Map showing the South Napa earthquake rupture traces (magenta lines) in relation to surficial geology and the mapped traces of ancient bedrock faults and faults previously mapped as part of the West Napa Fault System (black dashed lines are well-defined faults; dotted where concealed or inferred). Trace A (see fig. 19) is generally coincident with a fault that juxtaposes early Cretaceous and late Jurassic Great Valley Sequence rocks with late Eocene or early Miocene Domengine Sandstone; note how trace A bends to the northeast in the Browns Valley neighborhood to conform to the trend of this fault. Trace E (fig. 19) is partly coincident with a bedrock fault that juxtaposes the Domengine Sandstone with late Miocene to Pliocene Sonoma Volcanics. In contrast, trace C (fig. 19) is mostly not associated with previously mapped faults, but it does intermittently show geomorphic evidence of prior recent faulting. Trace F (fig. 19) at the Napa County Airport occurred along a mapped trace of the West Napa Fault Zone that was categorized under the Alquist-Priolo Fault Zoning Act. Geologic base map generalized from Wagner and Gutierrez (2010). Qhe, late Holocene estuarine (bay mud) deposits, includes large areas of fill over bay mud and salt layers. Qha, undifferentiated Holocene and modern alluvial deposits; includes stream terrace, fan, and channel deposits. Qpa, undifferentiated Pleistocene to early Holocene alluvial fan and terrace deposits, and colluvium. Th, early Pleistocene Huichica Formation consisting of gravel, sand, reworked tuff, and clay. Tsv, undifferentiated Sonoma Volcanics (late Miocene to Pliocene). Tm, undifferentiated San Pablo Group and marine sandstone and mudstone of Miocene age. Td, Domengine Sandstone (late Eocene or early Miocene). Tc, Eocene Capay Shale; KJgv, undivided Great Valley Sequence (late Jurassic to early Cretaceous).

The surface rupture associated with this earthquake is unusually large for an earthquake of M_w 6.0. Table 3 compares seismological and surface faulting parameters of the *M*6.0 August 24, 2014, South Napa earthquake with 11 other moderate magnitude (in the range of *M*6) strike-slip earthquakes that have occurred in California since 1948. These earthquakes show a range of behavior with regard to the occurrence and amount of coseismic surface faulting and afterslip. For example, the M_L5 Galway Lake earthquake, which is the smallest event in the data set, was associated with 6.8 km of surface faulting, while the M_w 6.2 Morgan Hill earthquake had no coseismic surface rupture.

Of these 12 moderate magnitude earthquakes, the 2014 South Napa earthquake has the longest coseismic surface rupture (≥12.5 km) and largest coseismic surficial displacement (a combined ≥60 cm from traces A, C, and E). The surface rupture was also unusually complex, involving surface slip on at least five distinct fault traces distributed across a 2 km-wide zone, whereas most other similar sized earthquakes involved surface slip on only one fault trace or no surface slip at all.

Much of the surface rupture from the 2014 South Napa earthquake occurred coincident with or near mapped traces of ancient faults that juxtapose highly deformed Mesozoic and Tertiary rocks (fig. 21); in particular, parts of rupture traces A, E, and the northern part of C appear to be associated with these old structures. Clearly, the existing bedrock structure plays a major role in controlling the surface rupture character of the WNFS in this area. Geologists have observed geomorphic expressions of recent faulting along the main traces. The CGS (with NEHRP funding) was conducting additional fault hazard studies when the South Napa earthquake struck. This recent earthquake has focused attention on the complex nature of the WNFS and will undoubtedly result in a more detailed characterization of this fault zone.

Postearthquake observations of a consultant's trenches excavated across trace E demonstrate that prehistoric earthquakes have occurred on this fault trace (fig. 22). The August 24, 2014, rupture is a simple crack that extends to the surface. However, the zone of faulting (red lines) broadens with depth, and the stratigraphic units exposed in the wall of the trench show increasing displacement with depth. At least three paleoearthquakes, labeled as events 2, 3, and 4, can be identified (fig. 22). These field relations indicate that, at least along trace E, prior fault ruptures have had larger amounts of slip and therefore reflect a much longer rupture length than what occurred in 2014. This may be the case along

other rupture traces as well and opens the possibility that the many strands of the WNFS may all be active and part of a broad shear zone where surface displacements along the various traces may vary from earthquake to earthquake over time. Additionally, data from this trench suggest that future events on the fault system may be substantially larger than the M_w 6.0 that occurred in 2014.

Further geologic studies aimed at determining the slip rate and the timing of prehistoric earthquakes will need to be conducted in order to better constrain the seismic hazard of the fault traces that slipped in 2014, as well as on other Quaternary faults comprising the WNFS.

Table 3. Comparison of seismological and surface faulting parameters for ~*M*6 strike-slip earthquakes in California since 1948.

[Magnitude (*M*), magnitudes are *M*w unless noted as M_L. Source is UCERF 3 seismicity catalog (Felzer, 2013) unless otherwise noted. Focal Depth D (km), source is UCERF 3 seismicity catalog (Felzer, 2013) unless otherwise noted. Coseismic surface rupture length (km), reported length of rupture at the surface at time of event, distinct from afterslip. Where multiple fault traces occurred, length listed is for the longest trace. Coseismic Dmax, reported maximum coseismic surface displacement. Does not include afterslip. nr. not reported]

Event (year)	Magnitude (*M*)	Focal depth D (km)	Coseismic surface rupture length (km)	Coseismic Dmax at surface (cm)	Creep prior to event	Surface afterslip (cm)	Notes
Desert Hot Springs (1948)	6.0	6.0	0	0	no	nr	M and D (Felzer, 2013). Richter and others (1958) report no surface rupture; 18-km aftershock zone.
Galway Lake (1975)	5.0 M_L	5.8	6.8	1.5	no	nr	M and D (Felzer, 2013). Surface offset data from Hill and Beeby (1977).
Parkfield (1966)	6.0	8.6	0 (SA) 10 (SWFZ)	0 (SA) 6.6 (SWFZ)	yes	31 (SA)	M and D (Ellsworth, 1990). San Andreas creeping at 28 mm/yr. Afterslip along 44 km of main San Andreas (SA) Coseismic slip on Southwest Fracture Zone (SWFZ). Surface offset data from Lienkaemper and Prescott (1986).
Homestead Valley (1979)	4.8 M_L 5.5 4.5 M_L 4.8 M_L	8.3 9.3 8.9 2.0	3.25 (HV) 1.5 (JV)	11 1	no	nr	M and D (Felzer (2013). Earthquake swarm with rupture along Homestead Valley (HV) and Johnson Valley (JV) faults; both reruptured during 1992 *M*7.2 Landers event. Surface offset data from Hill and others (1980).
Coyote Lake (1979)	5.9	8.95	0	0	yes	0.5	M and D (Oppenheimer and others, 1990); 14-km rupture length at depth. Discontinuous surface cracking for 14.4 km is likely afterslip. Surface observations from Armstrong (1979).
Greenville (1980)	5.8	14.79	4-6	≥1	yes	≥1	M and D (Ellsworth, 1990). Pre-event creep at 1–2 mm/yr (Lienkaemper and others, 2014). Total surface slip (coseismic + afterslip) was 2.5 cm (Bonilla and others, 1980). Concurrent rupture of conjugate Las Positias fault.
Morgan Hill (1982)	6.2	8.42	0	0	yes	nr	M and D (Oppenheimer and others, 1990); 25-km rupture length at depth (between 4–10 km). No unequivocal coseismic surface rupture (Harms and others, 1987).
North Palm Springs (1986)	6.02	10.4	9	<0.1	no	nr	M and D (Felzer, 2013). Discontinuous, en-echelon, left-stepping fractures for 9 km along surface trace Banning strand of San Andreas (SA). Offset data from Sharp and others (1986) who refer to these as "trace fractures" and interpret them as incipient faulting.
Elmore Ranch (1987)	6.04	10.8	10	20	no	nr	M and D (Felzer, 2013). Slip distributed on six traces across 8.5-km-wide zone. Longest is 10 km (Elmore Ranch fault). Cumulative surface Dmax for all traces is 20 cm., average ~10 cm. Surface offset data from Hudnut and others (1989).
Joshua Tree (1992)	6.15	12.3	0	0	no	nr	M and D (Felzer, 2013). 1.5-km discontinuous, triggered slip on East Wide Canyon fault (Rymer, 2000).
Parkfield (2004)	6.0	7.9	0 (SA) 8 (SWFZ)	<0.2 (SA) 6.6 (SWFZ)	yes	13–36 SA	M and D (USGS). No measurable coseismic rupture on main San Andreas (SA) but followed by 32 km of discontinuous afterslip varying from 13–36 cm. Coseismic rupture on Southwest Fracture Zone (SWFZ). Offset data from Langbein and others (2006), Lienkaemper and others (2006).
South Napa (2014)	6.0	10.7	≥12.5	≥60	no	≥35	M and D (USGS). Rupture involved 5 fault traces; some may be triggered. Longest (western) is a minimum of 12.5 km. Afterslip on west trace, primarily along southern 8.5 km; value listed is after 60 days with afterslip ongoing. Coseismic Dmax combines strands A (46 cm), C (8 cm) and E (6 cm).

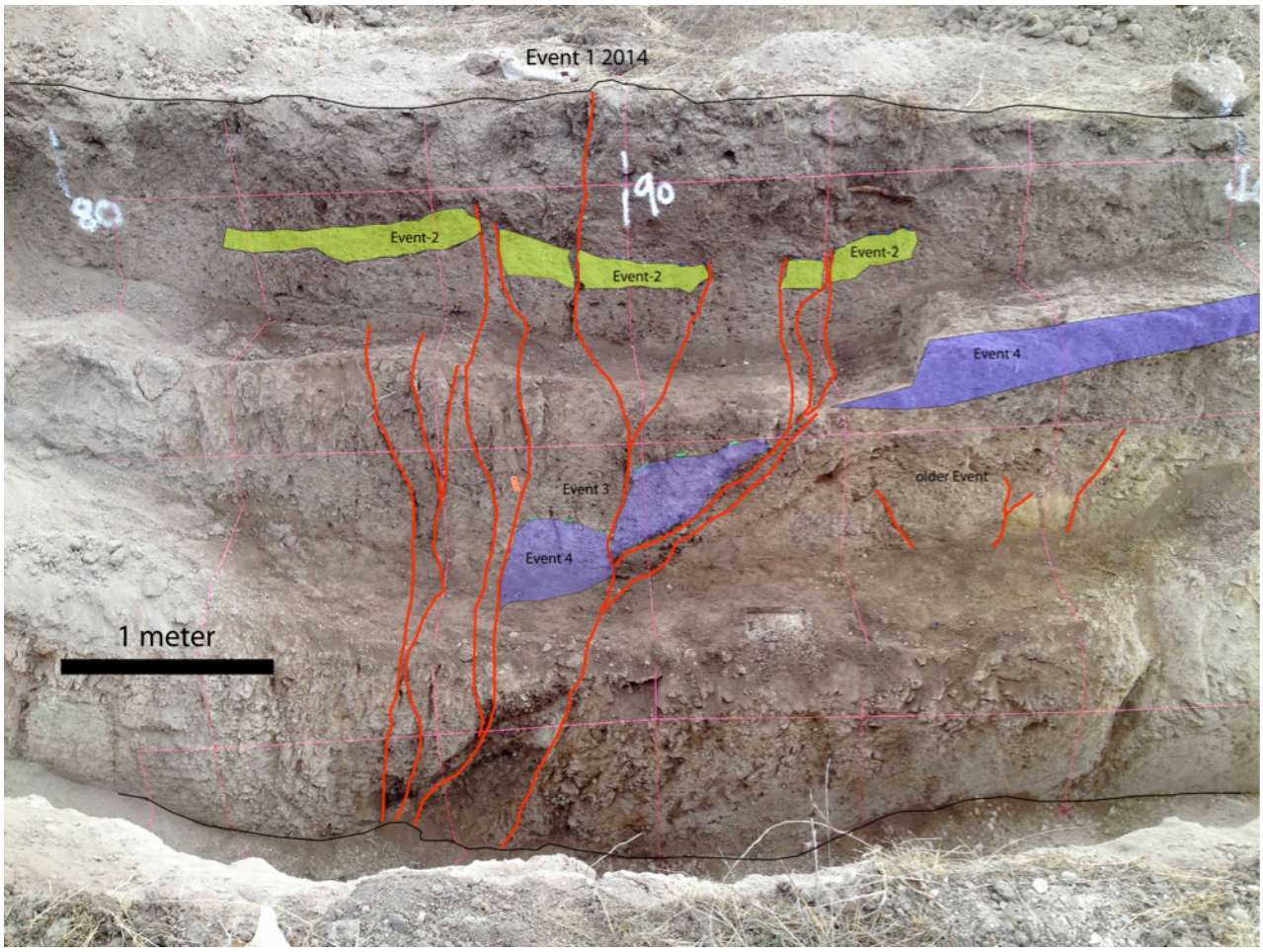

Figure 22. Annotated photograph showing the south wall of a trench cut across trace E near its southern end. Logging of this trench reveals that multiple, much larger displacements have occurred at this location in the past. Preliminary paleoseismic interpretations results indicate 3–4 earthquakes. Two key event horizons are denoted by yellow (Event 2) and blue (Event 4) shading. A distinct down-section increase in vertical separation across multiple fractures (red) is observed. In contrast, the 2014 surface rupture was expressed by a vertical down- to-the-left step of 1–3 cm along a single fracture. C-14 dating of these paleo earthquakes is pending. Photograph and interpretation by Gordon Seitz, CGS.

Critical Lifeline Infrastructure Impacts

The surface rupture and afterslip associated with the South Napa earthquake produced impacts on critical lifeline infrastructure in several notable locations along the fault breaks: (1) Between Cuttings Wharf and Highway 12, two gas main pipelines and a high-tension powerline withstood the coseismic and early afterslip offsets. (2) Highway 12 was offset and repaired repeatedly during ongoing afterslip, as were many other roads such as Old Sonoma Road. (3) Within Browns Valley, the utility service lines (water, power, etc.) to homes were disrupted by coseismic fault offsets. For at least 2 months after the earthquake, excavations made during repairs were temporarily covered by steel plates.

Two gas mains serve the northern San Francisco Bay Area, and one of these lines was temporarily decommissioned for repairs. The gas main is a 26-inch diameter line that normally operates at 350 pounds per square inch, and it runs adjacent to a school property. The line was temporarily excavated and happened to be exposed at the time of airborne LiDAR scanning on September 9, 2014. As an example of the fault offset and afterslip, figure 23 shows the airborne LiDAR data for this pipeline fault crossing location. The fault crosses the image at approximately the midpoint of this ~50-m exposed section of the gas main. Lifeline performance in future events, with both coseismic slip and afterslip, deserves additional consideration.

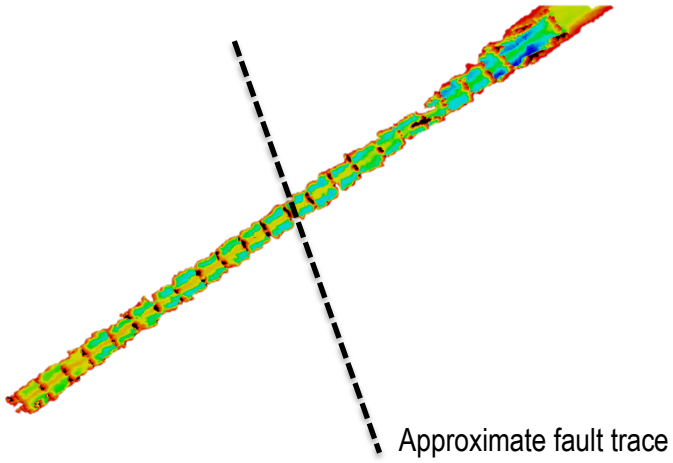

Figure 23. Diagram showing a gas pipeline crossing perpendicular to a fault. The gas main is the orange-yellow feature, which is subtly warped more than 35 cm by fault offset, most of which accumulated as afterslip that is still continuing as of 3 months after the earthquake.

Imagery

The U.S. Geological Survey operates a facility called the Earth Resources Observation and Science (EROS) Center that is located in Sioux Falls, South Dakota. This major facility houses the Hazard Data Distribution System (HDDS), which serves as the main repository and access point for pre- and postdisaster imagery collected from federal agencies and other sources. This imagery is available for domestic as well as global disasters through their support of the International Charter on Space and Major Disasters for a wide range of multihazard events, including anthropogenic disasters such as oil spills.

In the case of the South Napa earthquake, USGS has endeavored to work with partners to ensure that all important imagery acquired for documentation of the earthquake be placed onto the HDDS. The USGS encourages public domain access of the imagery, extending to multiple-purpose uses of the imagery to the greatest extent possible. Rapid, free, and open access to imagery is critical to the national approach to ensuring best use of geospatial information following disasters, and this is understood to be highly important for providing a more efficient overall response phase. USGS works with FEMA on an ongoing basis to ensure interoperability and complementary functionality between HDDS and other servers such as the FEMA HSIN and geoplatform.gov, as well as data.gov and other servers that

together form the network of resources available to emergency managers. USGS supports disaster-related exercises to ensure that its HDDS and other servers are functioning to support FEMA and others, for example, State agencies during disaster response and recovery.

The uniform resource locator (URL) for all imagery that USGS is serving on HDDS is *http://hddsexplorer.usgs.gov/*. For the South Napa earthquake holdings—high-resolution commercial electro-optical, LANDSAT, and other satellite and airborne imagery—please search on 201408_Earthquake_CA.

USGS Aerial and Ground-Based Photos

On August 25, 2014, the California Highway Patrol based at Napa County Airport performed an airborne mission and obtained a set of hand-held, stereo-overlapped aerial photographs from 250–300 m above ground using a digital, single-lens reflex camera (Canon EOS 70D) with an iPad running gpsRecorder and using a wireless GPS unit (Dual XGPS150). This collection was requested by USGS, with the fault rupture zone map and flightline guidance provided by USGS and CGS partners. These photographs, with metadata including georeferenced centers of these air photographs, may be accessed from the HDDS. Thousands more aerial and ground-based USGS photographs are also on the HDDS, and these provide important documentation of ephemeral earthquake damage, such as occurred to roads, that were repaired soon after the earthquake.

Contracted Aerial LiDAR and Photogrammetry Available from USGS

During numerous discussions among participants in the California Earthquake Clearinghouse, led by Anne Rosinski of CGS, a strong interest emerged in performing postearthquake airborne LiDAR and aerial photogrammetry along the fault rupture zone. Such imagery is considered essential for documentation of fault ruptures, ever since it was first performed after the 1999 Hector Mine earthquake (Hudnut and others, 2002). It is also recognized that pre-event, reference imagery is extremely useful so that pre- and postevent (before and after) imagery differencing may be performed to detect ground surface changes. This is an important way to observe earthquake effects and ground deformation (for example, Oskin and others, 2012). In the case of the South Napa earthquake, fortunately, pre-earthquake airborne LiDAR data had been acquired by the National Center for Airborne Laser Mapping (NCALM) during May 15 to June 1, 2003, for the Napa River Watershed survey, covering the area from Calistoga to San Pedro Bay (red polygon shown in figure 24).

Figure 24. LiDAR imagery coverage extent for the Napa Watershed from the National Center for Airborne Laser Mapping in 2003.

The Napa River Watershed LiDAR project is described in a detailed NCALM report, and the entire dataset is available.[13]

Recognizing that this presented a special opportunity to use differential LiDAR, the CGS, USGS, and PEER-GEER engineering group formed a partnership to ensure that postearthquake airborne LiDAR could be obtained. The Department of Water Resources (DWR), who had an existing contract with a commercial imagery provider and was willing to expedite and facilitate this important imagery acquisition, led this consortium. As a result of each partner paying their share of the costs, the acquisition was made possible on September 9, 2014. That dataset is described in a detailed report that, along with the raw data, metadata, and all of the deliverable files such as point clouds and DEMs, are hosted on HDDS. The extent of the LiDAR is shown in yellow and the extent of the stereo photographic coverage is shown in white in figure 25.

[13] *http://opentopo.sdsc.edu/gridsphere/gridsphere?gs_action=lidarDataset&cid=geonlidarframeportlet&opentopoID=OTLAS.052010.26910.1.*

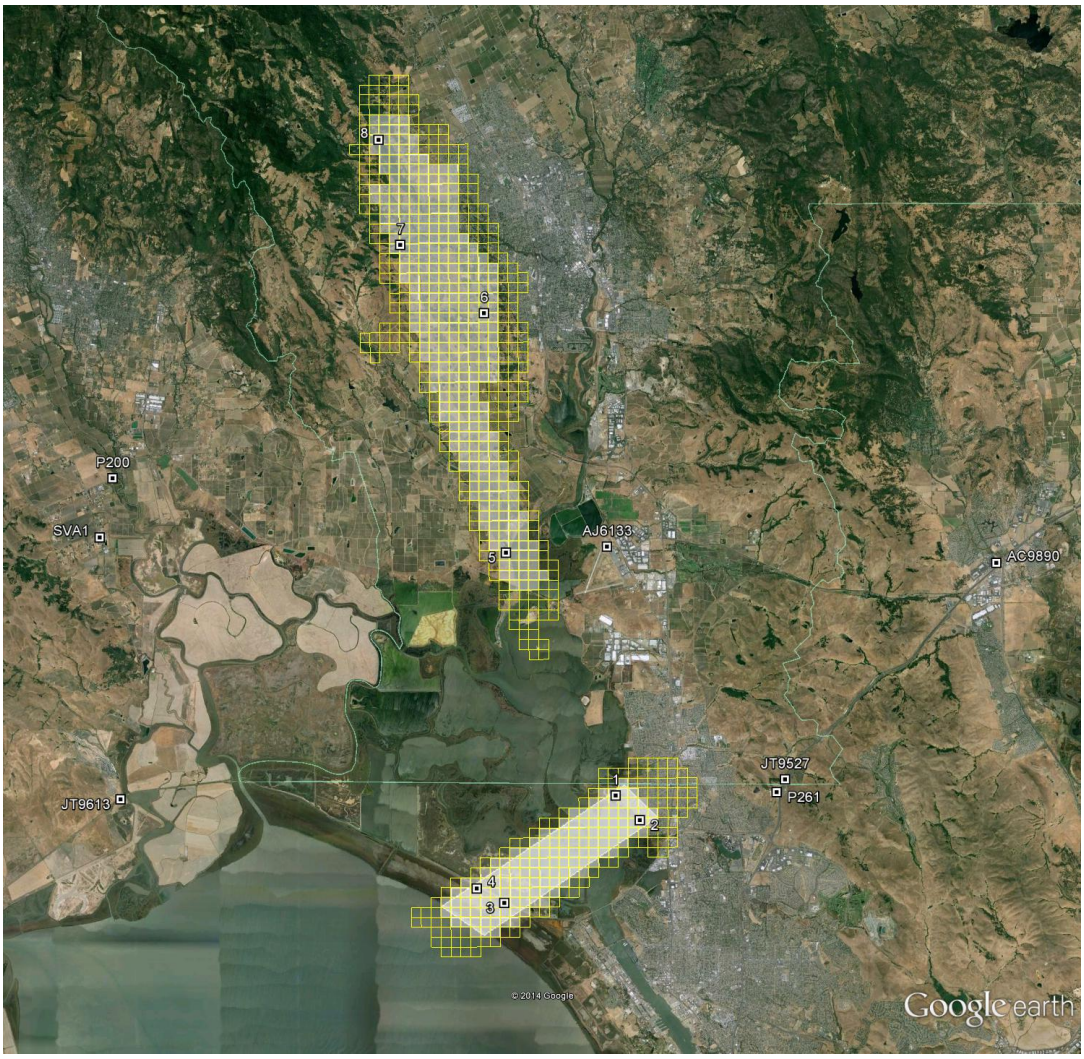

Figure 25. Google Earth image showing the GPS ground control network (includes UNAVCO PBO and other GPS stations, shown as white dots with black centers) and extent of the airborne LiDAR data (yellow crosshatch pattern) and stereo photographic coverage (white shaded). These data were acquired on September 9, 2014, to help document earthquake effects along the fault. County lines are also shown (thin green lines).

The airborne data were acquired using an Optech Orion M300 scanner, an Applanix 200 GPS-IMU, and a DiMac D-8900 ultralight medium format camera owned and operated by Towill, Inc., a California surveying and mapping firm. Ground control was performed, in part, with Trimble 5700 GPS units and zephyr antennas by Towill, who also incorporated data from nearby continuous PBO stations.

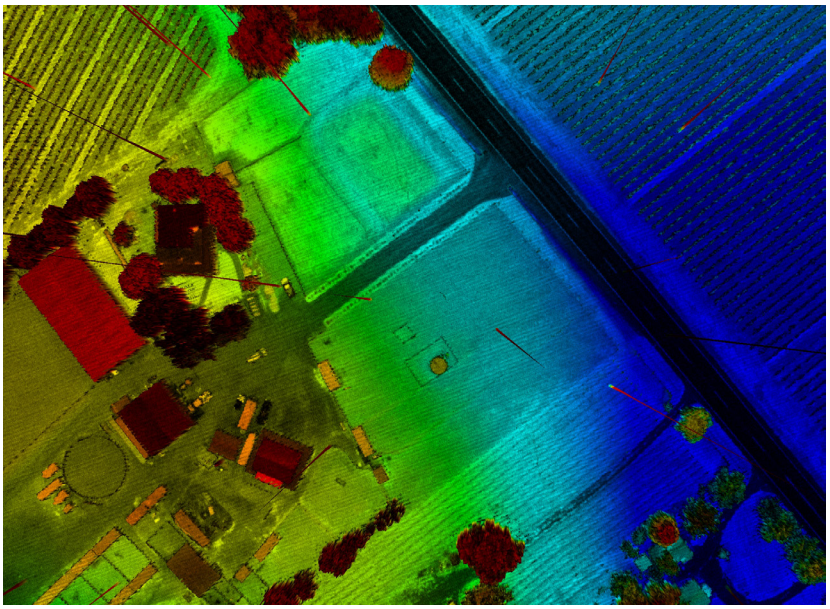

Figure 26. Example of September 9, 2014, LiDAR data showing a horse pasture south of Highway 12 and west of Cuttings Wharf Road. Fault rupture can be seen (faintly) where it crosses open ground, running from left of center at the top to right of center at the bottom. Blue to red color indicates elevation change, with blue indicating the lower elevation.

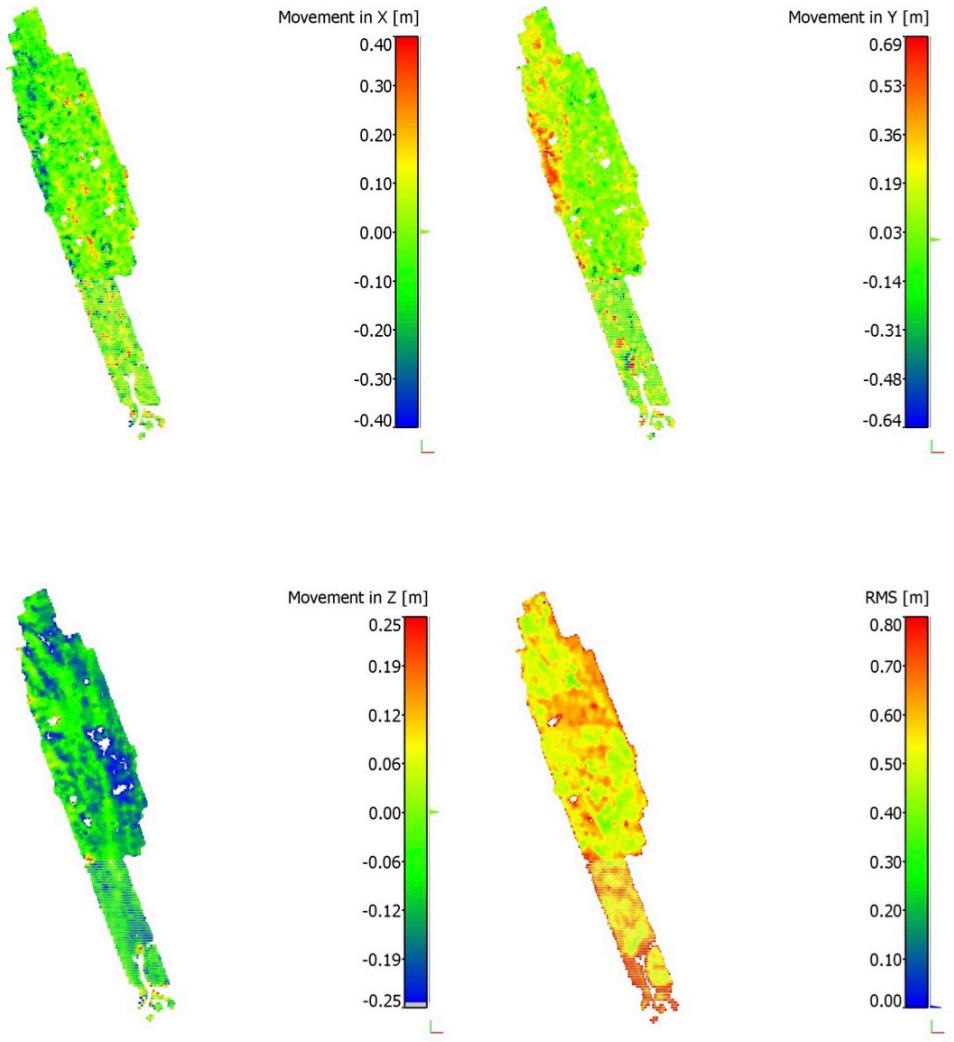

Figure 27. Image showing pre- to postearthquake LiDAR differences. Upper left panel is displacement in the east-west direction, upper right panel is displacement in the north-south direction, lower left panel is vertical displacement and lower right panel is error (root mean square). For the Browns Valley area, less than 5 cm of vertical displacement and less than 5 cm tilt is observed. Therefore, any changes in floodplain boundaries resulting from the earthquake deformation would likely be small, although this result is preliminary.

As a result of the timely acquisition of the airborne LiDAR and photos on September 9, 2014, it is now possible to compare pre- and postevent imagery in novel ways. Differencing of pre- and postevent imagery is complex and has required concurrent technique development. Although Oskin and others (2012) performed such differencing by one method, and other scientific literature has performed variations on this basic method, in the case of the South Napa earthquake, the ground deformation signal is rather small. Fortunately, however, the quality of the pre- and postearthquake LiDAR data is good.

The Oskin and others (2012) study was able to make use of sparse and lower quality pre-earthquake data, whereas in the South Napa case, we have far better quality pre-event LiDAR with which to perform the differencing. In this case, however, the ground deformation signal is much smaller than for the El Mayor-Cucapah earthquake studied by Oskin and others (2012). For these reasons, in the current study, we are innovating refinements of these proven differencing methods. In figure 27, initial and preliminary results are shown that are consistent with other information that we have obtained about the ground deformation in the South Napa earthquake.

We will continue to improve methods, but these initial findings may be immediately useful (although preliminary) for assessing the ground deformation in the residential areas near Browns Valley and Napa as well. Future applications may include other disaster recovery applications, for example, checking the levee system, earth fills, and engineered structures such as bridges.

Satellite and Other Imagery Available from USGS

The USGS and its partners acquired other satellite imagery, most of which was made publicly available on the USGS HDDS. In some cases, imagery acquired by USGS was purchased under restricted-access license and may not be made openly available. Imagery has proven useful, however, for describing the overall afterslip along the fault. In figure 28, an example Radarsat-2 image, processed by Chuck Wicks, is shown. To examine the afterslip, many dozens of InSAR and UAVSAR images were analyzed, but only selected examples are given in this report for the sake of brevity. A slide presentation of the afterslip imagery analysis used for developing the relevant portions of this report is available upon request.

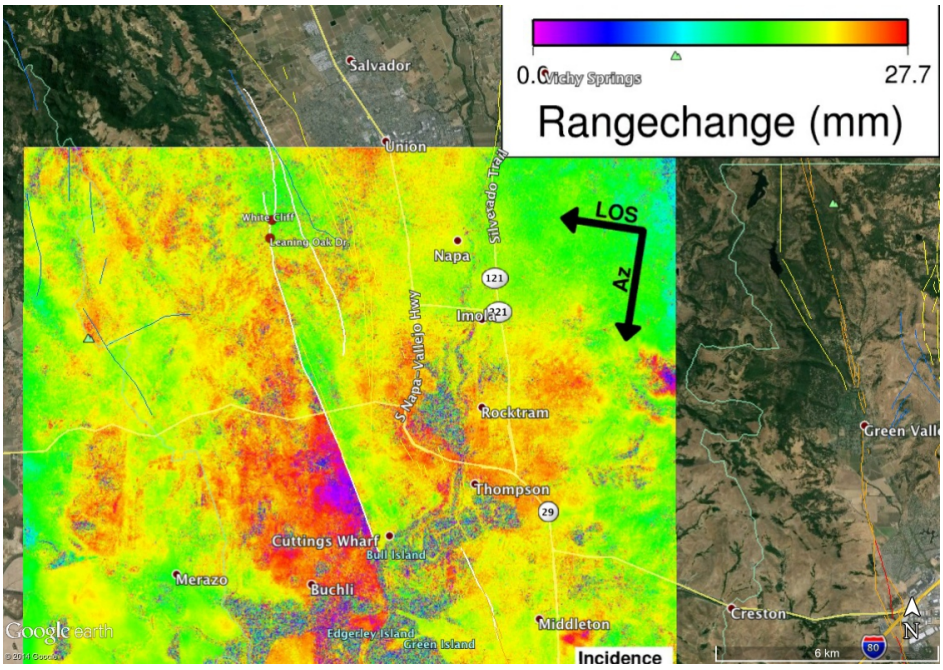

Figure 28. Radarsat-2 postseismic image for the time period September 9 through October 8, 2014, using a 2.77-cm color-wrap scale.

In addition to the various satellite and airborne SAR data examined to assess afterslip, a large amount of satellite and aerial imagery (in addition to the September 9, 2014, Towill contracted dataset) was acquired soon after the earthquake and is also available from HDDS. Figures 29–33 show coverage extents of the following: (1) a total of 1,576 stereo-overlapped, very high resolution (<5 centimeters per pixel) aerial photos acquired by California Highway Patrol on August 25, 2014, at the request of USGS (fig. 29); (2) high-resolution (0.5-meter) electro-optical imagery such as WorldView 2 and QuickBird 1 and 2 (figs. 30, 31); (3) medium-resolution electro-optical and multispectral imagery such as Landsat-8 and SPOT-6 (figs. 32, 33).

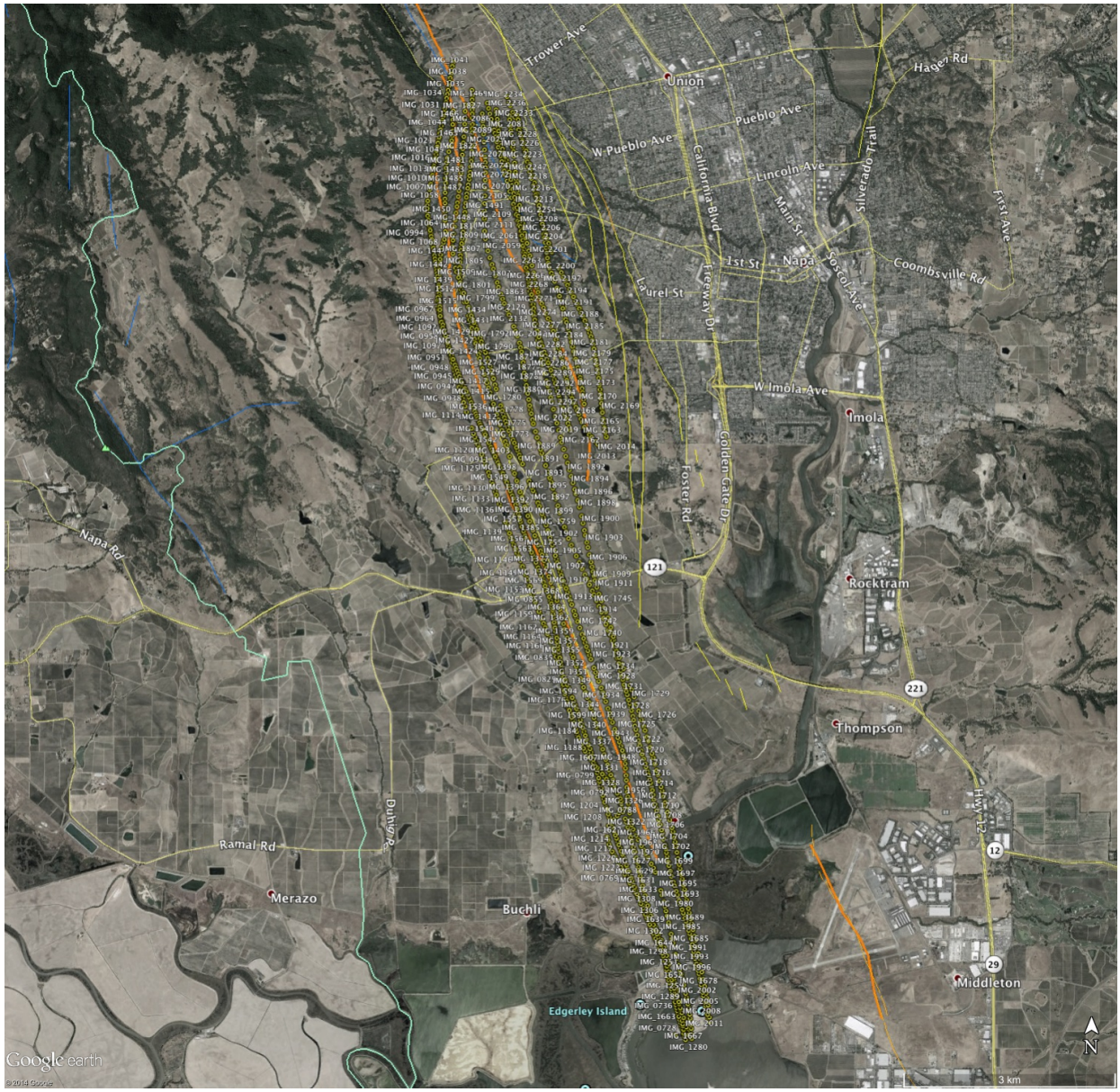

Figure 29. Photo map index showing the locations of aerial photographs acquired by California Highway Patrol at the request of USGS on August 25, 2014, for the main fault rupture zone. All images acquired by CHP are accessible at USGS Hazard Data Distribution System (HDDS). Orange line, main trace of West Napa Fault; white numbers are photo labels; green lines are county boundaries.

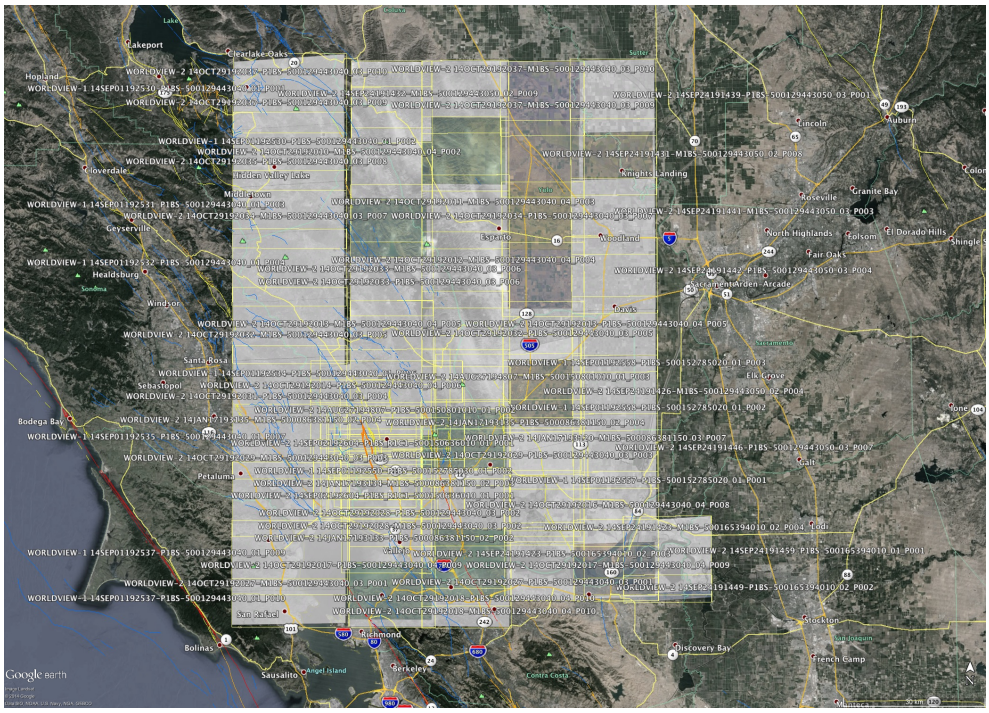

Figure 30. Coverage area of WorldView 1 and 2 high-resolution EO imagery scenes (white translucent block) available through USGS Hazard Data Distribution System (HDDS).

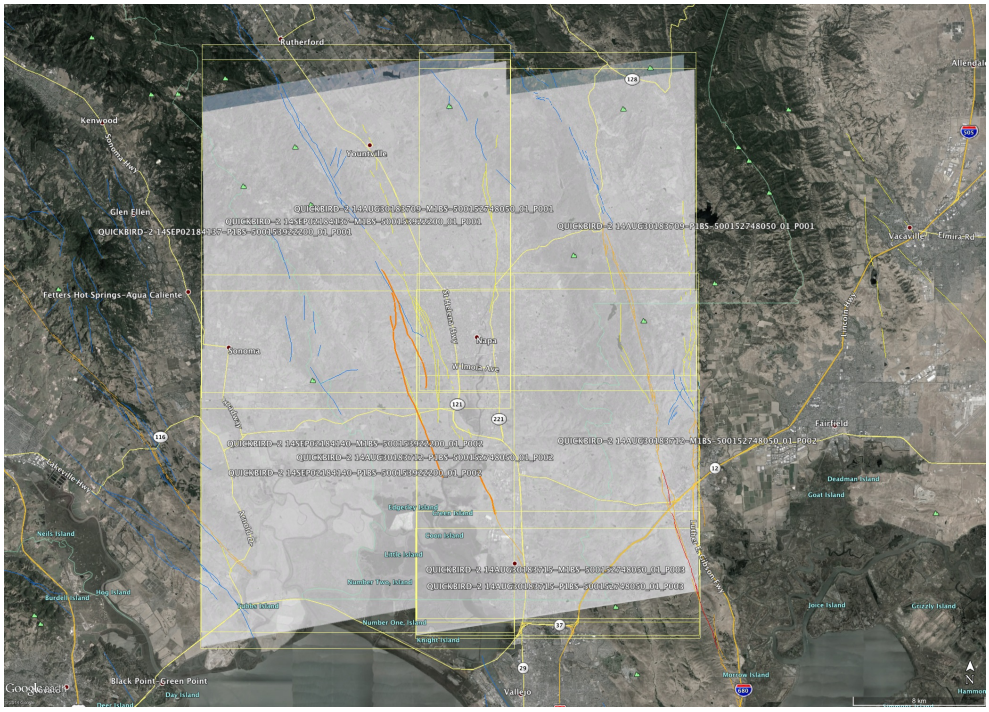

Figure 31. Coverage of QuickBird high-resolution EO imagery scenes available through USGS Hazard Data Distribution System (HDDS) for Napa, Calif., and surrounding area.

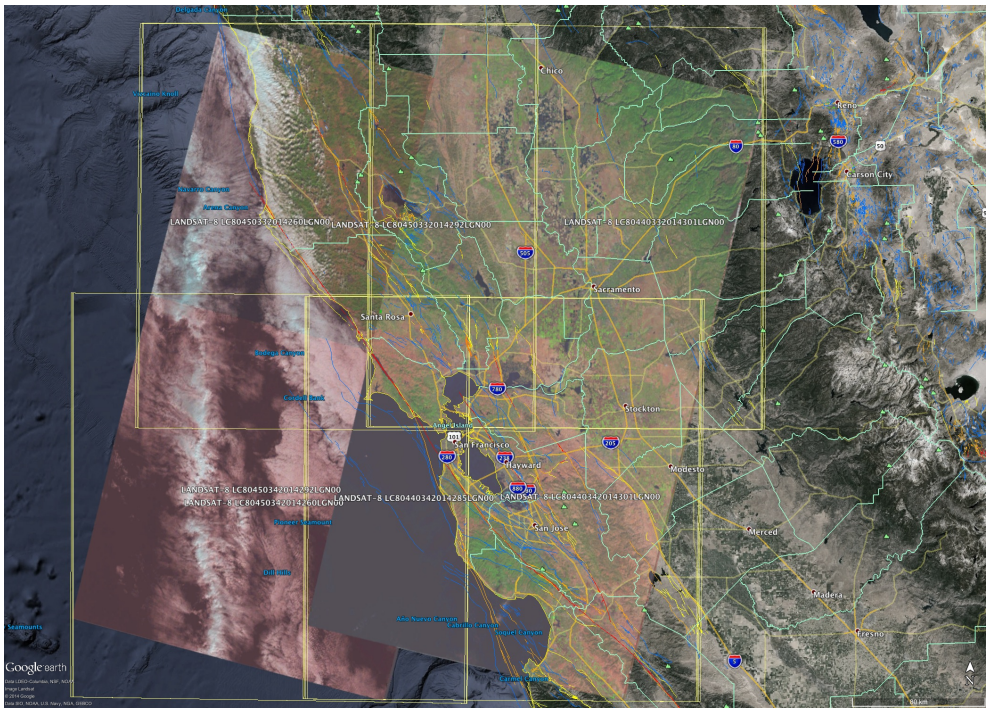

Figure 32. Coverage areas for Landsat-8 medium-resolution EO and multispectral imagery scenes, available through USGS Hazard Data Distribution System (HDDS).

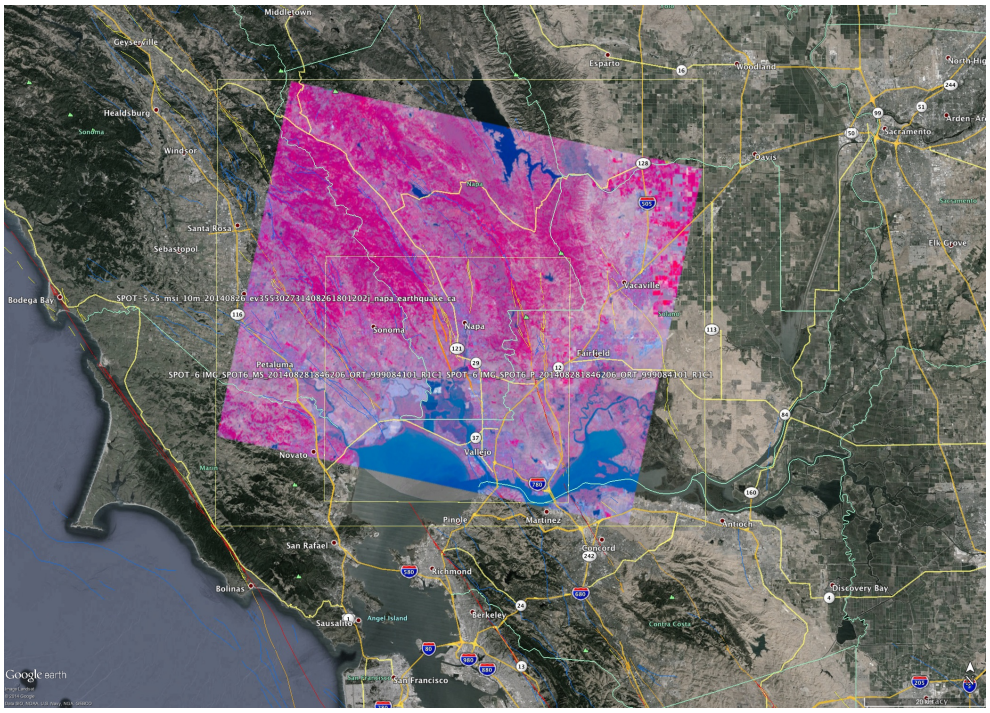

Figure 33. SPOT-6 medium-resolution EO and multispectral-resolution scenes (colored square shows coverage) available through USGS Hazard Data Distribution System (HDDS) for Napa, Calif., and surrounding area.

Conclusions and Closing Statements

The South Napa earthquake on August 24, 2014, produced instantaneous damage resulting from ground shaking and coseismic surface rupture, as well as permanent ground deformation. In addition, ongoing fault movement along the surface rupture, called afterslip, has produced further damage. Aftershocks have not been as energetic as is typical for California earthquakes, yet these aftershocks clearly pose an ongoing hazard. This report focuses on the fault afterslip in the Browns Valley neighborhood, as well as the shaking pattern in the downtown area of the City of Napa. Imagery that has already been collected is also presented, as are initial findings that have resulted from preliminary postprocessing of some of the imagery, such as the pre- and postearthquake airborne LiDAR data. Preliminary findings on fault hazards from the eastern strand of the West Napa Fault System (fig. 19, trace E) indicate past earthquakes (as yet not dated) occurred prior to the 2014 earthquake that produced larger fault offsets and were therefore evidently bigger than the 2014 event on that trace. Imagery acquisition and postprocessing, as well as ongoing fieldwork on the fault hazards and differential LiDAR aspects of the project, will continue.

In December 2014, many scientists will present their latest findings about this earthquake at special sessions of the American Geophysical Union in San Francisco. Others who are not coauthors of this report may present findings that would be of interest to FEMA, CalOES, the County and City of Napa, and especially to residents of the impacted region. Additional future relevant findings, either by ourselves or others, may help to better explain the situation or further alleviate the uncertainty surrounding the future afterslip, aftershocks, and other aspects of the ongoing earthquake-related hazards in the vicinity of the August 24, 2014, earthquake and the impacted surrounding area.

References Cited

Aagaard, B.T., Graves, R.W., Rodgers, A., Brocher, T.M., Simpson, R.W., Dreger, D., Petersson, N.A., Larsen, S.C., Ma, S., and Jachens, R.C., 2010, Ground motion modeling of Hayward fault scenario earthquakes, Part II—Simulation of long-period and broadband ground motions: Bulletin of the Seismological Society of America, v. 100, no. 6, p. 2945–2977, doi: 10.1785/0120090379.

Armstrong, C.F., 1979, Coyote Lake earthquake, August 6, 1979: California Geology, v. 32, no. 11, p. 248–251.

Beyzaei, C., Bray, J., Cohen-Waeber, J., Dawson, T., Harder, L., Hudnut, K., Kelson, K., Kishida, T., Lanzafame, R., Luque, R., Ponti, D., Shriro, M., Sitar, N., Wagner, N., and J. Wesling, J., 2014, Geotechnical Engineering Reconnaissance of the August 24, 2014 M6 South Napa Earthquake [Version 1]: Geotechnical Extreme Events Reconnaissance Association, Report No. GEER-037, accessed November 20, 2014, at *http://www.geerassociation.org/GEER_Post%20EQ%20Reports/SouthNapa_2014/index.html.*

Boatwright, J., 2014, Rupture directions for selected northern California earthquakes:U.S. Geological Survey Web page, accessed: November 18, 2014, at *http://earthquake.usgs.gov/research/rupture/*.

Boatwright, J., Seekins, L.C., Fumal, T.E., Liu, H.-P., and Mueller, C.S., 1991, Ground motion amplification in the Marina District: Bulletin of Seismological Society of America, v. 81, p. 1980–1997.

Boatwright, J., Budding, K.E., Sharp, R.V., 1989, Inverting measurements of surface slip on the Superstition Hills fault, Bulletin of Seismological Society of America, v. 79, p. 411–423.

Bonilla, M.G., Lienkaemper, J.J., and Tinsley, J.C., 1980, Surface faulting near Livermore, California, associated with the January 1980 earthquakes, U.S. Geological Survey Open-File Report 80-523: U.S. Geological Survey, 27 p.

Budding, K.E., Boatwright, J., Sharp, R.V., and Saxton, J.L., 1989, Compilation and analysis of displacement measurements obtained on the Superstition Hills fault zone and nearby faults in Imperial Valley, California, following the earthquakes of November 24, 1987: U.S. Geological Survey Open-File Report 89-140, 90 p.

Donnellan, A., Parker, J., Hawkins, B., Hensley, S., Jones, C., Owen, S., Moore, A., Pierce, M., Wang, J., and Rundle, J., 2014, Combined UAVSAR and GPS Estimates of Fault Slip for the M 6.0 South Napa Earthquake [abs.]: American Geophysical Union, 2014 Fall Meeting abstract #S31G-04, *https://agu.confex.com/agu/fm14/meetingapp.cgi#Paper/32711*.

Earthquake Engineering Research Institute, 2014, M6.0 South Napa, California Earthquake: California Earthquake Clearinghouse Web site, accessed November 18, 2014, at *https://www.eeri.org/2014/08/m6-0-south-napa-california-earthquake-california-earthquake-clearinghouse/*.

Ellsworth, W.L., 1990, Earthquake History, 1769–1989, chap. 6 *of* Wallace, R.E., ed., The San Andreas fault system, California: U.S. Geological Survey Professional Paper 1515, p. 152–187.

Felzer, K.R., 2013, The UCERF3 earthquake catalog, appendix K *in* Field, E.H., and others, Uniform California earthquake rupture forecast, version 3 (UCERF3)—The time-independent model: USGS Open-File Report 2013–1165, CGS Special Report 228, and Southern California Earthquake Center Publication 1792, *http://pubs.usgs.gov/of/2013/1165/pdf/ofr2013-1165_appendixK.pdf/*.

Field, E.H., Arrowsmith, R.J., Biasi, G.P., Bird, P., Dawson, T.E., Felzer, K.R., Jackson, D.D., Johnson, K.M., Jordan, T.H., Madden, C., Michael, A.J., Milner, K.R., Page, M.T., Parsons, T., Powers, P.M., Shaw, B.E., Thatcher, W.R., Weldon II, R.J., and Zeng, Y., 2014, Uniform California Earthquake Rupture Forecast, Version 3 (UCERF3)—The Time-Independent Model: Bulletin of the Seismological Society of America, v. 104, no. 3, p. 1122–1180.

Graves, R.W., Pitarka, A., and Somerville, P.G., 1998, Ground-motion amplification in the Santa Monica area: Effects of shallow basin-edge structure, Bulletin of Seismological Society of America, v. 88, p. 1224–1242.

Hill, R.L., Treiman, J.A., Given, J.W., Pechman, J.C., McMillan, J.R., and Ebel, J.E., 1980, Geologic study of the Homestead Valley earthquake swarm of March 15, 1979: California Geology, v. 33, no. 3, p. 60–67.

Harms, K.K., Clark, M.M., Rymer, M.J., Bonilla, M.G., Harp, E.L., Herd, D.G., Lajoie, K.R., Lienkaemper, J.J., Mathieson, S.A., Perkins, J.A., Wallace, R.E., and Ziony, J.I., 1987,The search for surface faulting, chap. 7 *of* Hoose, S.N., ed., The Morgan Hill, California, earthquake of April 2, 1984: U.S. Geological Survey Bulletin 1639, p. 61–68.

Housner, G.W., 1959, Behavior of structures during earthquakes: Journal of Applied Mechanics, Division American Society of Civil Engineers, Proceedings Paper 2220, v. 85, EM4, p. 109–129.

Hudnut, K.W., Seeber, L., and Rockwell, T., 1989, Slip on the Elmore Ranch fault during the past 330 years and its relation to slip on the Superstition Hills fault: Bulletin of the Seismological Society of America, v. 79, no. 2, p. 330–333.

Hudnut, K.W., Borsa, A., Glennie, C., and Minster, J.-B., 2002, High-resolution topography along surface rupture of the 16 October 1999 Hector Mine, California, earthquake (Mw7.1) from airborne laser swath mapping: Bulletin of the Seismologial Society of America, v. 92, no. 4, p. 1570–1576, 2002.

Langbein, J., Murray, J.R., and Snyder, H.A., 2006, Coseismic and initial postseismic deformation from the 2004 Parkfield, California, earthquake, observed by global positioning system, electronic distance meter, creepmeters, and borehole strainmeters: Bulletin of the Seismological Society of America, v. 96, no. 4b, p. S304–S320, doi:10.1785/0120050823.

Lienkaemper, J.J., and W.H. Prescott, 1986, Historic surface slip along the San Andreas Fault near Parkfield, California: Journal of Geophysical Research, v. 94, no. B12, p. 17647–17670.

Lienkaemper, J.J., Baker, B., and McFarland, F.S., 2006, Surface slip associated with the 2004 Parkfield, California, earthquake measured on alinement arrays: Bulletin of the Seismological Society of America, v. 96, no. 4B, p. S239–S249, doi:10.1785/0120050806.

Lienkaemper, J.J., Brooks, B.A., DeLong, S.B., Domrose, C.J., and Rosa, C.M., 2014, Surface slip associated with the 2014 South Napa, California earthquake measured on alinement arrays [abs.]: American Geophysical Union, 2014 Fall Meeting abstract #S33F-4898, *https://agu.confex.com/agu/fm14/meetingapp.cgi - Paper/32688/.*

Montesi, L.G.J., 2004, Controls of shear zone rheology and tectonic loading on postseismic creep: Journal of Geophysical Research, v. 109, doi: 10.1039/2003JB002925.

Oppenheimer, D.H., Bakun, W.H., and Lindh, A.G., 1990, Slip partitioning of the Calaveras fault, California, and prospects for future earthquakes: Journal of Geophysical Research, v. 95, no. B6, p. 8483–8498.

Oskin, M.E., Arrowsmith, J.R., Hinojosa-Corona, A., Elliott, A.J., Fletcher, J.M., Fielding, E.F., Gold, P.O., Gonzalez Garcia, J.J., Hudnut, K.W., Kreylos, O., and Teran, O., 2012, Surface rupture complexity of the El Mayor-Cucapah earthquake quantified by airborne LiDAR: Science, v. 335, no. 6069, p. 702–705, doi: 10.1126/science.1213778.

Perfettini. H., and Avouac, J.-P., 2004, Postseismic relaxation driven by brittle creep—A possible mechanism to reconcile geodetic measurements and the decay rate of aftershock, application to the Chi-Chi earthquake, Taiwan: Journal of Geophysical Research, v. 109, no. B2, doi: 10.1029/2003JB002488.

Richter, C.F., Allen, C.R., and Nordquist, J.M., 1958, The Desert Hot Springs earthquakes and their tectonic environment: Bulletin of the Seismological Society of America, v. 90, p. 315–337.

Rymer, M.J., 2000, Triggered surface slips in the Coachella valley area associated with the 1992 Joshua Tree and Landers, California, earthquakes: Bulletin of the Seismological Society of America, v. 48, no. 4, p. 832–848.

Sharp, R.V., Rymer, M.J., and Morton, D.M., 1986, Trace fractures on the Banning fault created in association with the 1986 North Palm Springs earthquake: Bulletin of the Seismological Society of America, v.76, no. 6, p. 1838–1843.

U.S. Geological Survey and California Geological Survey, 2006, Quaternary fault and fold database for the United States: U.S. Geological Survey Web site, accessed October 15, 2014, at *http://www.earthquake.usgs.gov/hazards/qfaults/*.

Wagner, D.L., and Gutierrez, C.I., 2010, Preliminary geologic map of the Napa 30’ x 60’ Quadrangle, California: California Geological Survey, scale 1:100,000.

Witter, R.C., Knudsen, K.L., Sowers, J.M., Wentworth, C.M., Koehler, R.D., and Randolph, C.E., 2006, Regional Quaternary Geology: U.S. Geological Survey Open-File Report 2006–1037.

Vidale, J.E., and Helmberger, D.V., 1988, Elastic finite-difference modeling of the 1971 San Fernando, California earthquake: Bulletin of the Seismological Society of America, v. 78, p. 122–141